Nerve and Blood Vessels

4

Maura Valle and Maria Pia Zamorani

CONTENTS

M. Valle, MD
Staff Radiologist, Reparto di Radiologia, Istituto Scientifico "Giannina Gaslini", Largo Gaslini 5, 16148 Genova, Italy
M. P. Zamorani, MD
Unité de Recherche et Dévelopement, Clinique des Grangettes, 7, ch. des Grangettes, 1224 Genève, Switzerland

4.1 Nerve

4.1.1 Histologic Considerations

From the histologic point of view, nerves are round or flattened cords, with a complex internal structure made of myelinated and unmyelinated nerve fibers, containing axons and Schwann cells grouped in fascicles (Fig. 4.1a) (Erickson 1997). Along the course of the nerve, fibers can traverse from one fascicle to another and fascicles can split and merge. Based on the fascicular arrangement, two theories have been hypothesized to explain the internal architecture of a nerve: the "cable" and the "plexiform" models (Stewart 2003). The first states that nerves are cable-like structures, in which fascicles run separately throughout the entire nerve length (Fig. 4.1b). The second asserts that fascicles alternate splitting, branching, and rejoining along the course of the nerve trunk (Fig. 4.1c). In fact, nerves have both cable and plexiform arrangement of the fascicles depending on the level of examination. In their more proximal portion (e.g., brachial plexus), a plexiform organization of the fascicles predominates. More distally (e.g., median nerve), nerves present a cable-like structure with high degree of somatic organization (e.g., sensory and motor fibers for a specific area of the skin or muscle contained in the same fascicle) (Stewart 2003). The nerve tissue is embedded in a series of connective tissue layers.

A closer look at the nerve sheaths demonstrates an external sheath – the outer epineurium – which surrounds the nerve fascicles. Each fascicle is invested in turn by a proper connective sheath – the perineurium – which encloses a variable number of nerve fibers and is responsible for the "blood-nerve" barrier. Then, the individual nerve fibers are invested by the endoneurium. The connective tissue intervening between the outer nerve sheath and the fascicles is commonly referred to as the interfascicular

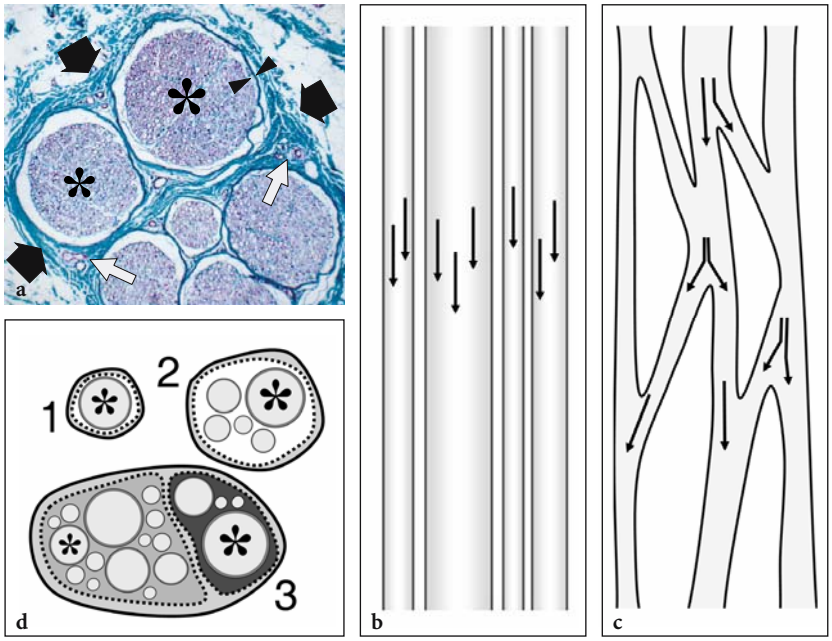

Fig. 4.1a–d. Nerve histology. **a** Histologic cross-sectional view of the human sural nerve (*black arrows*) reveals some nerve fascicles (*asterisks*) of different size containing nerve tissue (*violet*) with collections of axons, myelin sheaths, and Schwann cells. Individual fascicles are invested by a thin sheath – the perineurium (*arrowheads*) – and are separated from each other by a loose connective tissue envelope – the epineurium (*green*) – containing small intraneural vessels (*white arrows*). Specimen stained using the van Gieson procedure (original magnification ×150). **b,c** Schematic drawings of a long-axis view through the nerve trunk illustrate the models of fascicular organization. *Arrows* indicate the axonal path. **b** In the "cable model," the fascicles run parallel to the nerve axis without axonal exchange. **c** In the "plexiform model," fascicles split and rejoin in various combinations with axons intermingling from one to another. **d** Schematic drawing of a cross-sectional view of the monofascicular (*1*), oligofascicular (*2*), and polyfascicular (*3*) nerve models. In complex motor and sensory nerves (*3*), fascicles (*asterisks*) are of different size and may be grouped in function-related areas within the nerve. This drawing (*3*) recalls the structure of the sciatic nerve, in which the nerves fibers for the tibial nerve (*light gray*) and for the peroneal nerve (*dark gray*) remain grouped tightly throughout the course of the nerve, even proximally

epineurium (internal epineurium), as opposed to the outer epineurium which surrounds the entire nerve trunk. Generally speaking, the amount of connective tissue of the epineurium is more abundant in large multifascicular nerves and in regions in which the nerve is mobile across joints (Delfiner 1996). This thickening of the connective tissue seems to provide more cushioning for the nerve and, therefore, more resistance to compression injury (Delfiner 1996). Externally, the outer (external) epineurium is continuous with the mesoneurium, which is made up of loose areolar tissue. This latter structure is credited with not only supplying the framework for the blood supply entering the nerve, but also making the excursion of the nerve in its bed easier without traction on its blood supply during joint motion (George and Smith 1996).

Nerves have a prominent vascular supply to ensure their continuous supply of local energy required for impulse transmission and axonal transport. The vascular supply is formed by an interconnected system of perineural vessels that course longitudinally in the external epineurium and branch among the fascicles (endoneural vessels).

4.1.2 Normal US Anatomy and Scanning Technique

Thanks to the latest generation of high-frequency "small parts" transducers and compound technology, US has become a well-accepted and widespread imaging modality for evaluation of peripheral nerves. The improved performance of these transducers has made it possible to recognize subtle anatomic details at least equal to or even smaller than those depicted with surface-coil MR imaging and to depict a wide range of pathologic

conditions affecting nerves (Martinoli et al. 1999; Keberle et al. 2000; Beekman and Visser, 2004). Apart from the availability of high-end technology, nerve US requires thoughtful knowledge of anatomic details and close correlation of imaging findings with the patient's clinical history and the results of electrophysiologic studies. With these credentials, US provides low-cost and noninvasive imaging, speed of performance, and important advantages over MR imaging, including a higher spatial resolution and the ability to explore long segments of nerve trunks in a single study and to examine nerves in both static and dynamic states with real-time scanning.

The US appearance of normal nerves is fairly uniform, closely reflecting their histologic composition (Fig. 4.2) (Silvestri et al. 1995). On short-axis planes, US demonstrates nerves as honeycomb-like structures composed of hypoechoic spots embedded in a hyperechoic background in which the hypoechoic structures correspond to the fascicles that run longitudinally within the nerve, and the hyperechoic background relates to the interfascicular epineurium (Figs. 4.2a, 4.3a) (Silvestri et al. 1995). This pattern somewhat resembles the section of an electric cable. On long-axis planes, nerves typically assume an elongated appearance with multiple hypoechoic parallel linear areas, which correspond to the neuronal fascicles that run longitudinally within the nerve, separated by hyperechoic bands (Fig. 4.3b) (Silvestri et al. 1995). In an individual nerve, the size and number of the fascicles may vary depending on the distance from site of origin, the amount of pressure to which the nerve is subjected, and the occurrence of nerve branching (Fig. 4.1d). In nerve bifurcations, for instance, the nerve trunk divides into two or more secondary nerve bundles, whereas fascicles enter only one of the divisional branches without splitting. The outer boundaries of nerves are usually undefined as they have a similar hyperechoic appearance to their connective envelopes, including the outer epineurium, the mesoneurium, and the surrounding loose connective spaces, all of which contain fat. In normal states,

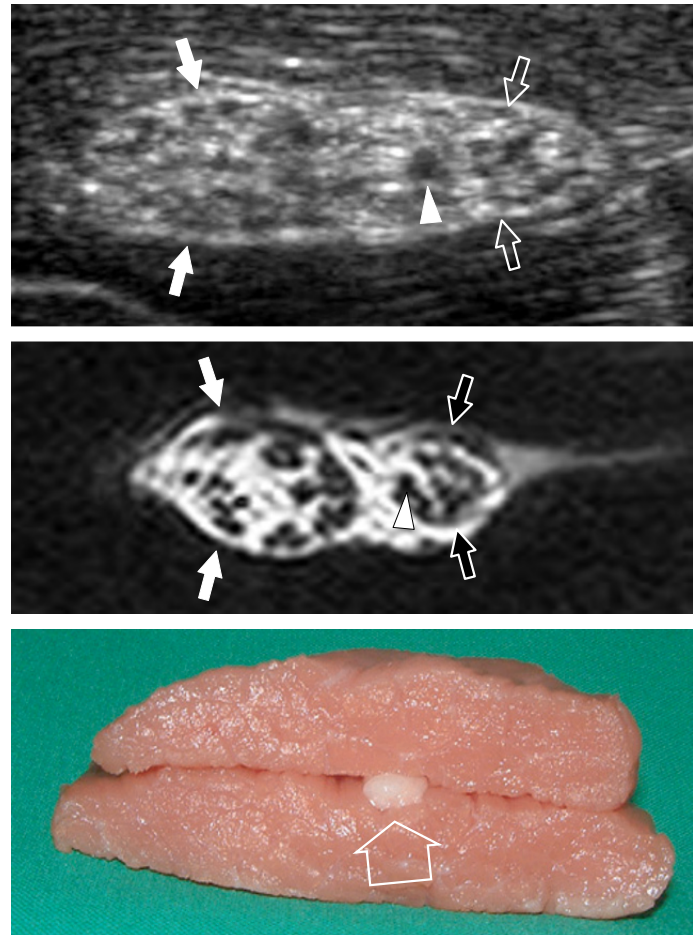

Fig. 4.2a–c. Nerve anatomy. In vitro **a** short-axis 12–5 MHz US image of the bovine sciatic nerve (*arrows*) with **b** correlative T1-weighted MR imaging demonstrates a honeycombed nerve echotexture made up of small rounded hypoechoic areas (*arrowhead*), the fascicles, that are embedded in a hyperechoic background, the epineurium. Observe the definite grouping of fascicles within the sciatic nerve for the tibial (*white arrows*) and the peroneal (*open arrows*) nerves. **c** The in vitro model was prepared by incorporating the nerve (*open arrow*) within muscle tissue

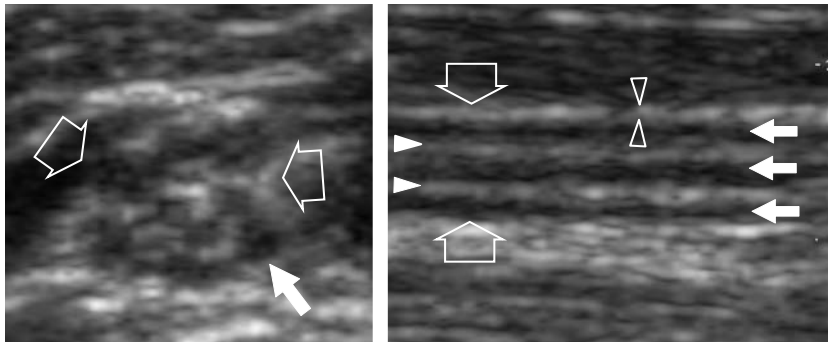

Fig. 4.3a,b. Normal nerve echotexture. **a** Short-axis and **b** long-axis 15–7 MHz US images over the median nerve (*open arrows*) at the mid-forearm. In **a**, the nerve fascicles (*white arrow*) are depicted as well-circumscribed individual structures of different size separated by echogenic epineurium. In this segment, 11 fascicles are distinguished in the cross-sectional area of the median nerve. In **b**, the nerve fascicles appear as elongated hypoechoic bands (*white arrows*) that run parallel to each other. The internal epineurium (*white arrowheads*) separates them more clearly, while the external epineurium (*open arrowheads*) helps to define the outer boundaries of the nerve

color and power Doppler systems are, for the most part, unable to recognize the weak and small blood flow signals from the perineural plexus and the intraneural branches. Generally speaking, nerves are compressible and alter their shape depending on the volume of the anatomic spaces within which they run as well as on the bulk and conformation of the perineural structures (Fig. 4.4a,b). Even with slight pressure applied with the probe, they may be seen sliding over the surface of an artery or a muscle. As a general rule, each individual fascicle in a nerve runs independently of the others. Across synovial joints, they pass through narrow anatomic passageways – the osteofibrous tunnels – that redirect their course. The floor of these tunnels consists of bone, whereas the roof is made of focal thickenings of the fascia – the retinacula – that prevent dislocation and traumatic damage of the structures contained in the tunnel during joint activity (Martinoli et al. 2000b). When nerves cross tight passages, such as neural foramina and osteofibrous tunnels, subtle echotextural changes can be seen, with a more homogeneous hypoechoic appearance caused by tighter packing of the fascicles and local reduction in the volume of the epineurium (Sheppard et al. 1998).

A careful scanning technique based on the precise knowledge of their position and analysis of their anatomic relationships with surrounding structures is essential for recognizing peripheral nerves with US. Unlike other structures of the musculoskeletal system, nerves do not show anisotropic properties. Therefore, appropriate probe orientation during scanning is not needed to image them; however, systematic scanning in the short-axis plane is preferred for following the nerves contiguously throughout the limbs (Martinoli et al. 1999). Long-axis scans are less effective for this purpose because the elongated fascicles may be easily confused with echoes from muscles and tendons coursing along the same plane. Once detected, the nerve is kept in the center of the US image in its short axis and then followed proximally and distally, shifting the transducer up or down according to the nerve's course. With this technique – which we can call the "lift technique" – the examiner is able to explore long segments of a nerve in a few seconds throughout the limbs and extremities (Fig. 4.4c). If intrinsic or extrinsic nerve abnormalities are encountered during scanning, the US examination is then appropriately focused on the region of interest using oblique and longitudinal US scanning planes. Although all main nerves can be readily displayed in the extremities due to their superficial position and absence of intervening bone, depiction of the peripheral nervous system is not possible everywhere with US. In fact, most cranial nerves – except for the vagus – and the spinal accessory nerve (Giovagnorio and Martinoli, 2001; Bodner et al. 2002a), the nerve roots exiting the dorsal, lumbar and sacral spine, the sympathetic chains, and the splanchnic nerves in the abdomen cannot be visualized due to their course being to deep or interposition of bony structures. In addition, the perineural structures greatly influence nerve detection in the limbs and extremities. When nerves course deeply, as in obese patients, their evaluation can be difficult. As a general rule, nerves of the lower extremity run deeper than those of the upper extremity and are more difficult to visualize. Nerves coursing among hypoechoic muscles are

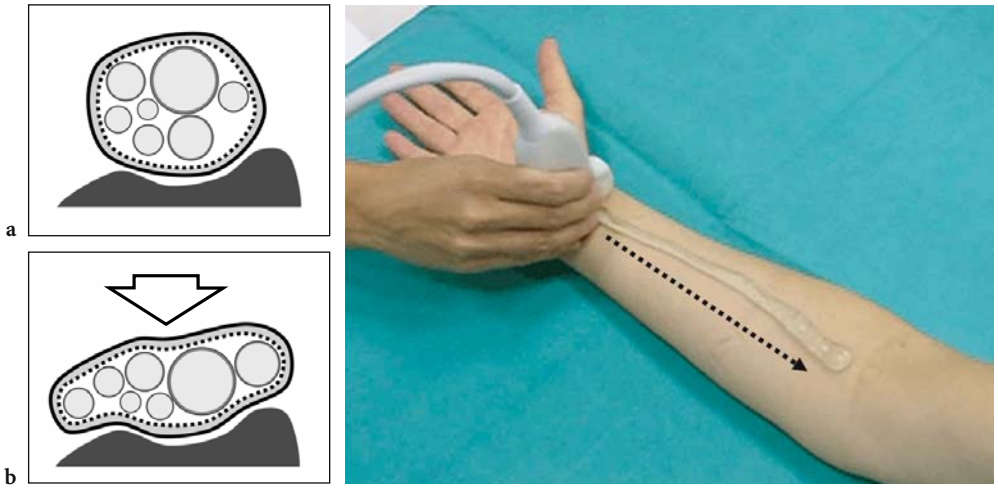

Fig. 4.4a–c. Response to compression and nerve scanning technique. **a,b** Schematic drawings of the cross-sectional view of a nerve lying over a stiff surface (bone) **a** at rest and **b** during external compression (*arrow*). Due to the flexibility of the epineurial sheath, the nerve flattens, whereas the fascicles – which are noncompressible structures – redistribute according to the nerve shape changes. **c** Photograph shows the standard technique for examining nerves in the limbs. The short axis of the median nerve at the wrist is centered in the field of view of the US image. Then, the transducer is swept upward (*dashed arrow*) along the course of the nerve in the forearm. This technique, which we can call the "lift technique," allow a simple and reliable evaluation of long nerve segments in a single sweep, excluding possible intrinsic and extrinsic abnormalities along the nerve path. The ability of US to follow the entire course of nerves in the limbs so quickly is a major advantage over MR imaging

detected easier than those surrounded by hyperechoic fat. Similarly, a nerve of a young physically active subject is better depicted than the same nerve examined in a subject with atrophic muscles.

4.1.3 Anatomic Variants, Inherited and Developmental Anomalies

Given the characteristic US appearance of normal nerves, some anatomic variants can be recognized with this technique. Among these, the proximal bifurcation of the median nerve at wrist has been extensively reported in the literature (see Chapter 10) (Propeck et al. 2000; Iannicelli et al. 2000; Gassner et al. 2002). Similarly, some inherited and developmental anomalies of the peripheral nervous system, such as the fusiform enlargement of the median nerve by fibrofatty tissue (so-called fibrolipomatous hamartoma), the hypertrophy of nerves in Charcot-Marie-Tooth syndrome (Martinoli et al. 2002), and the focal enlargement of nerves in hereditary neuropathy with liability to pressure palsies (Beekman and Visser 2002) can be recognized with US. In these disorders, US findings may contribute to the understanding of pathophysiology by noninvasively revealing some important morphologic information. Further work is, however, required to fully analyze the impact and reliability of US in this field.

4.1.3.1 Fibrolipomatous Hamartoma

Fibrolipomatous hamartoma is a developmental tumor-like nerve disorder related to the hypertrophy of mature fat and fibroblasts in the epineurium that often presents during early childhood. This condition – which is also referred to as neural fibrolipoma, perineural lipoma, fatty infiltration of the nerve, lipofibroma, or neural lipoma – has a definite predilection for the median nerve and its branches, with lower extremity involvement (plantar nerve, sciatic nerve) reported as being rare (Marom and Helms 1999; Wong et al. 2006). Fibrolipomatous hamartoma may be associated with local gigantism of an extremity, usually the hand or foot, related to bony overgrowth, fat proliferation in the soft tissues, and nerve-territory-oriented macrodactyly, characteristic of the condition known as macrodystrophia lipomatosa (Amadio et al. 1988; Murphey et al. 1999). The US appearance of fibrolipomatous hamartoma is pathognomonic of this entity, reflecting the morphology of the lesion. US demonstrates a

striking fusiform enlargement of the median nerve at the distal forearm through the palm, characterized by an increased bulk of hyperechoic adipose tissue in the epineurium that surrounds and is interposed between normal-appearing fascicles (Fig. 4.5a–d) (Murphey et al. 1999; Chen et al. 1996). At the carpal tunnel level, the affected median nerve may become symptomatic earlier than other nerves due to its encroachment by the flexor retinaculum. In these instances, detection of nerve fascicles that appear focally swollen within the adipose mass indicates compression and the need for carpal tunnel release (Fig. 4.5e–g). Debulking of the mass may compromise the intraneural vasculature causing catastrophic motor and sensory deficits or an intense healing response that may further jeopardize function (Marom and Helms 1999).

4.1.3.2 Charcot-Marie-Tooth Disease

Charcot-Marie-Tooth disease is a complex and heterogeneous group of inherited disorders of the peripheral nervous system, also known as hereditary motor and sensory neuropathies, that is characterized by hypertrophied peripheral neuropathy due to the abnormal growth (like an onion bulb) of Schwann cells (Fig. 4.6a,b). The most common clinical features include unsteady gait due progressive distal weakness of peroneal muscles, pes cavus, depressed or absent deep tendon reflexes, and mild sensory loss. The histopathologic abnormalities involve all nerves in the body and occur predominantly in the fascicles. Although the classification system of Charcot-Marie-Tooth disease is

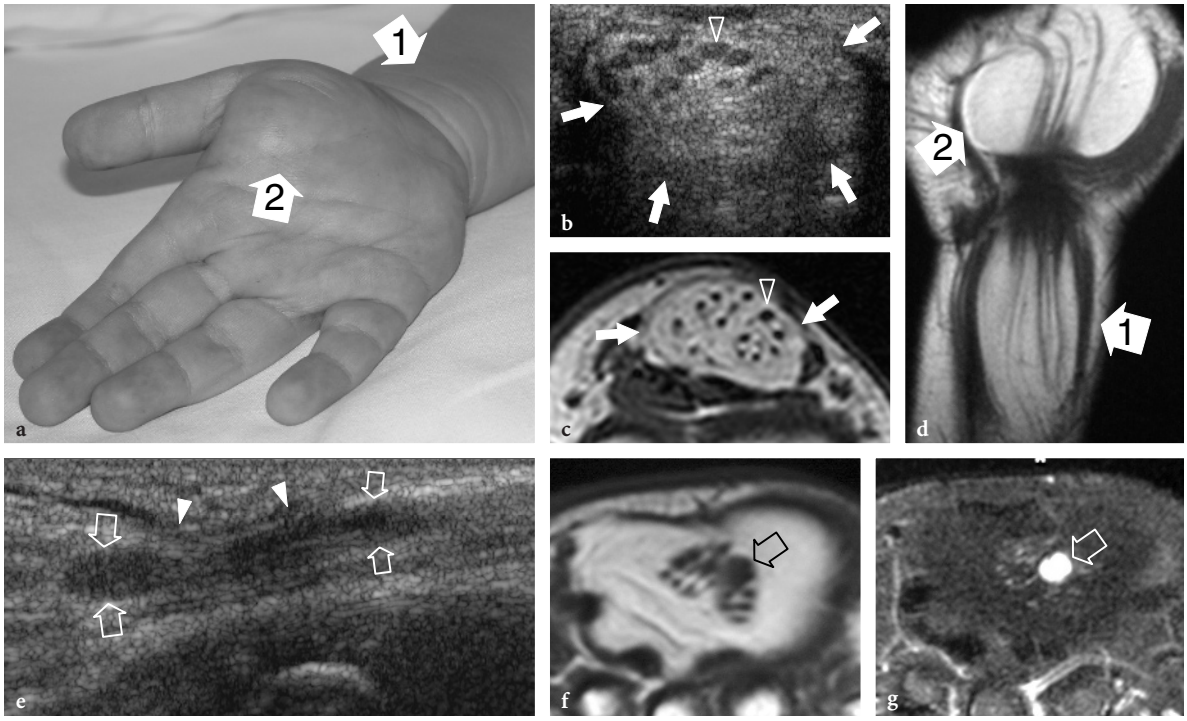

Fig. 4.5a–g. Fibrolipomatous hamartoma. **a** Photograph of the right hand of a 3-year-old child presenting with mild symptoms of median neuropathy and diffuse soft-tissue swelling and tenderness extending from the distal radius (*1*) through the radial aspect of the palm (*2*). **b** Transverse 12–5 MHz US image obtained proximal to the carpal tunnel with correlative **c** transverse and **d** coronal T1-weighted MR images demonstrates abnormal fusiform enlargement of the median nerve (*arrows*). The nerve exhibits normal-appearing fascicles (*arrowhead*) interspersed with hyperechoic fat in the epineurium. There is close correlation between the US and MR imaging findings. In the coronal plane, MR imaging demonstrates abnormal predominant fat growth outside the confined space of the carpal tunnel. **e** Longitudinal 12–5 MHz US image at the carpal tunnel level identifies fusiform swelling of an individual fascicle (*arrows*) just deep to the flexor retinaculum (*arrowheads*). Corresponding transverse **f** T1-weighted and **g** fat-suppressed T2-weighted MR images confirm the presence of a single swollen T2-hyperintense fascicle (*arrow*), compared with the adjacent normal ones, possibly indicating a compressive abnormality. The patient experienced relief of symptoms postoperatively and the pain did not recur during 1 year of postoperative follow-up

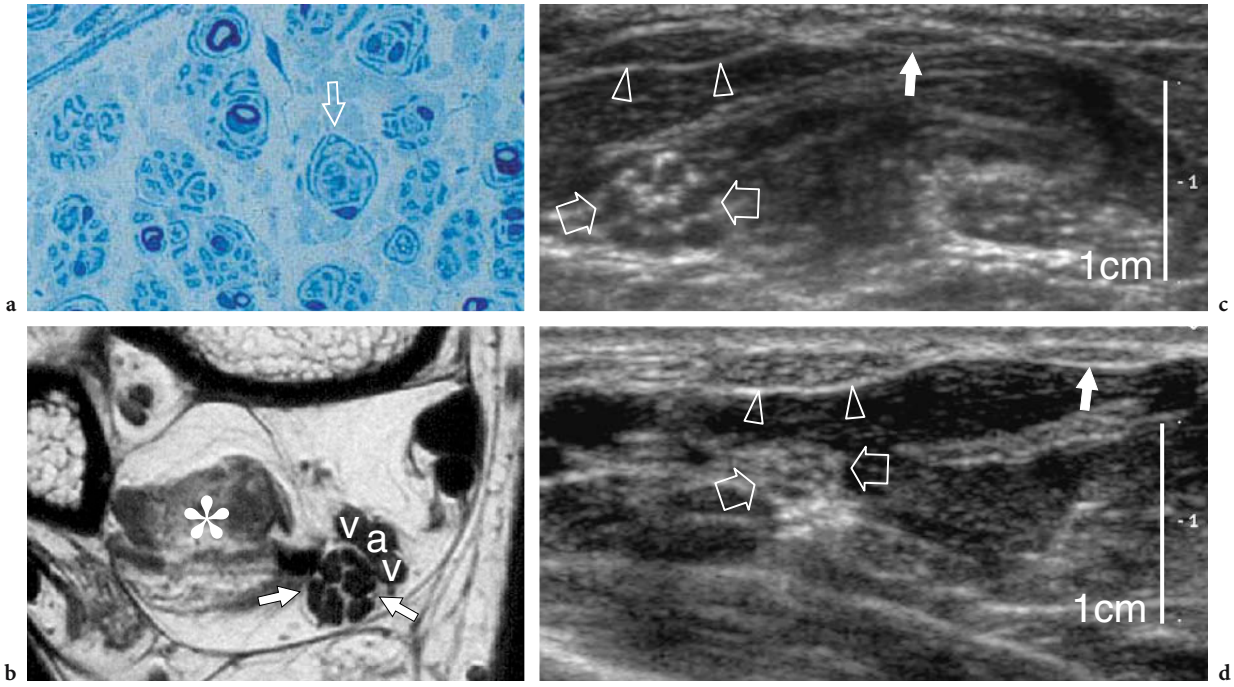

Fig. 4.6a–d. Charcot-Marie-Tooth disease in a 37-year-old woman with type 1A disease. **a** Histologic slice of a fascicle of the sural nerve demonstrates the abnormal "onion bulb" appearance (*arrow*) of the Schwann cells, a peculiar finding of Charcot-Marie-Tooth disease. Original magnification ×800. **b** Transverse T1-weighted MR image of the posterior ankle reveals an enlarged tibial nerve (*arrows*) characterized by swollen fascicles. The nerve is much larger than normal. Note the atrophic changes in the flexor hallucis longus muscle (*asterisk*) and the adjacent posterior tibial artery (*a*) and veins (*v*). **c** Short-axis 12–5MHz US image over the middle forearm reveals hypertrophy of the median nerve (*open arrows*) and its fascicles. **d** Corresponding 12–5 MHz US image of the median nerve obtained for comparison in a healthy woman at the same magnification shown in **c** demonstrates a smaller median nerve (*open arrows*) and fascicles. Note the equivalent size of the flexor carpi radialis (*arrowheads*) and palmaris longus (*white arrow*) tendons in the two images. The magnification scale is indicated on the *right*

constantly changing (because not all the causative genes have yet been described), the most common forms include the autosomal dominant types 1A and 2 that are related to DNA duplication of a region on chromosome 17 which codes for a peripheral myelin protein, and the X-linked type that is related to a mutation in the gene which codes for connexin 32, which is a gap-junction protein (Schenone and Mancardi 1999). The degree of electrophysiologic alterations varies widely among patients with different forms of the disease, especially in the type 1A, as a result of phenotypic differences and the action of stochastic factors or environmental modulation of disease severity (Schenone and Mancardi 1999). Nerves appear larger than normal but retain a normal fascicular echotexture (Heinemeyer and Reimers 1999; Martinoli et al. 2002). In considering the main genetic types of Charcot-Marie-Tooth disease, such as the autosomal dominant types 1A and 2, and the X-linked type, patients with type 1A have markedly larger fascicles than patients with the other disease subtypes. In these patients, the diameter of the fascicles and the resulting nerve area are more than twice those seen in healthy subjects and in type 2 and the X-linked type (Fig. 4.6c,d) (Martinoli et al. 2002). There is no correlation between the maximum fascicular size of the nerve and electrophysiologic features, such as distal latencies, velocities, and amplitude (Martinoli et al. 2002). In this specific clinical setting, US can be used to help the neurologist identify unrecognized disease in patients with nonspecific symptoms, to differentiate the 1A genetic subtype, and to provide a useful screening tool for a first selection of the individuals in an affected kindred who are to undergo genetic assessments.

4.1.3.3 Hereditary Neuropathy with Liability to Pressure Palsies

Hereditary neuropathy with liability to pressure palsies, also known as tomaculous neuropathy, is

an autosomal dominant inherited disorder characterized by a tendency to develop focal neuropathies after trivial trauma that is related to a deletion in chromosome 17p11.2-12 producing reduced expression of peripheral myelin protein 22 (Verhagen et al. 1993). Histopathologically, a sausage-shaped myelin sheath swelling, the so-called tomacula, is responsible for multifocal nerve enlargement. Electrophysiologic studies demonstrate one or more entrapment neuropathies on a background of motor and sensory polyneuropathy. The more frequently involved nerves are: the peroneal nerve at the fibular tunnel, the ulnar nerve at the cubital tunnel, the radial nerve at the spiral groove, and the median nerve at the carpal tunnel (Verhagen et al. 1993; Beekman and Visser 2002). US is able to recognize focal nerve enlargement not only at the osteofibrous tunnels that are typically involved, but also along the course of nerves throughout the limbs (Fig. 4.7). It is conceivable that the "sausage-shaped" myelin swellings (tomacula) found at teased nerve fiber studies in patients with this disorder are responsible for nerve enlargement (Beekman and Visser 2002).

4.1.4 Nerve Instability

Dynamic US of the elbow can be used to help demonstrate abnormal dislocation of the ulnar nerve, with or without snapping triceps syndrome. This finding typically occurs in the cubital tunnel, an osteofibrous tunnel formed by a groove between the olecranon and the medial epicondyle and bridged by the Osborn retinaculum. As described in Chapter 8, dynamic scanning during full elbow flexion can allow continual depiction of the intermittent dislocation of the ulnar nerve over the medial epicondyle if the retinaculum is loose or absent (Jacobson et al. 2001). Dislocation of the medial edge of the triceps can also occur in combination with dislocation of the ulnar nerve (Jacobson et al. 2001). In this syndrome, the ulnar nerve dislocation is secondary to the snapping triceps and dynamic scanning demonstrates the medial head of the triceps and the ulnar nerve remaining in close continuity as they dislocate over the medial epicondyle (see Chapter 8).

4.1.5 Compressive Syndromes

From a general pathophysiologic point of view, nerve compression can occur acutely or develop chronically. Short periods of constriction result in slowing and failure of conduction across the constriction point, whereas the nerve portion distal to the region that was compressed retains a normal function. The conduction abnormalities, which are generally referred to by the term "neuroapraxia," tend to resolve but there may be a prolonged latency until full recovery. This type of injury typically occurs in the radial nerve at the spiral groove of the humerus, the so-called "Saturday night radial palsy", and in the peroneal nerve around the fibular head and neck, the so-called "crossed leg peroneal palsy". If local compression is prolonged, ischemia induced by direct severe compression, mechanical distortion of the nerve architecture, may cause more significant damage in the myelin sheath and axonal degeneration (Wallerian degeneration) of the nerve fibers and persistent nerve deficit due to disruption of the axoplasm after the compression has been relieved (Delfiner 1996). In chronic nerve

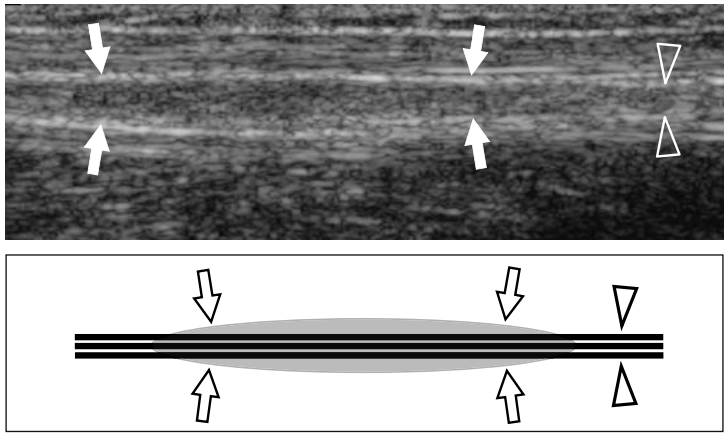

Fig. 4.7a,b. Hereditary neuropathy with liability to pressure palsies in a 42-year-old man with mild median and ulnar neuropathy. **a** Long-axis 12–5 MHz US image of the ulnar nerve (*arrowheads*) at the middle forearm with **b** schematic drawing correlation reveals mild fusiform thickening (*arrows*) of the nerve out of osteofibrous tunnels

entrapment, irritation or compression to the nerve may induce interference with the intraneural microvascular supply and an ischemic reaction primarily affecting the epineurium. Venous congestion may produce endoneural edema with increased fluid pressure within the environment of the fascicles, thereby inducing a microcompartment syndrome (Shon 1994; Delfiner 1996). In the early stages, symptoms may be intermittent or even relieved after exercise, parallel to recovery of the intraneural circulation and drainage of intraneural edema. As the disease progresses, the sustained edema of the epineurium may turn into fibrotic changes with thickening and fibrosis of the nerve sheaths, further contributing to a chronic constriction of the nerve. Longstanding compression leads to damage to the myelin sheath and axonal degeneration induced by fibrosis, with permanent loss of nerve function and atrophy of the innervated muscles. Nerve trunks that are compressed chronically are typically thin at the site of compression (with reduction in the number of myelinated fibers) and swollen proximal to the compression point. The physiologic consequences related to chronic compression are slowing of conduction velocities and, occasionally, conduction block.

4.1.5.1 Nerve Entrapment Syndromes

Nerve involvement from extrinsic causes may occur anywhere in the body. However, it is more common at anatomic sites where the nerve passes in unextensible osteofibrous tunnels or beneath a prominent or abnormal band of muscle, connective tissue, or bony ridge that tethers the nerve. Diagnostic assessment of nerve compressive syndromes is essentially based on clinical features and electrophysiologic testing, and the main value of imaging is in the assessment of difficult or atypical cases, or when a mass is suspected on clinical grounds. In recent years, US has increasingly been proposed as an efficient and low-cost alternative to MR imaging for detection of compressive lesions.

In nerve entrapment syndromes, US can demonstrate changes in both nerve shape and echotexture, the most common being a sudden flattening (notch sign) with focal reduction in the nerve cross-sectional area at the compression point and nerve swelling that occur proximal to the level of compression (Fig. 4.8) (Buchberger et al. 1991; Martinoli et al. 2000b). The nerve swelling is typically fusiform, extending 2–4 cm in length, and appears maximal in

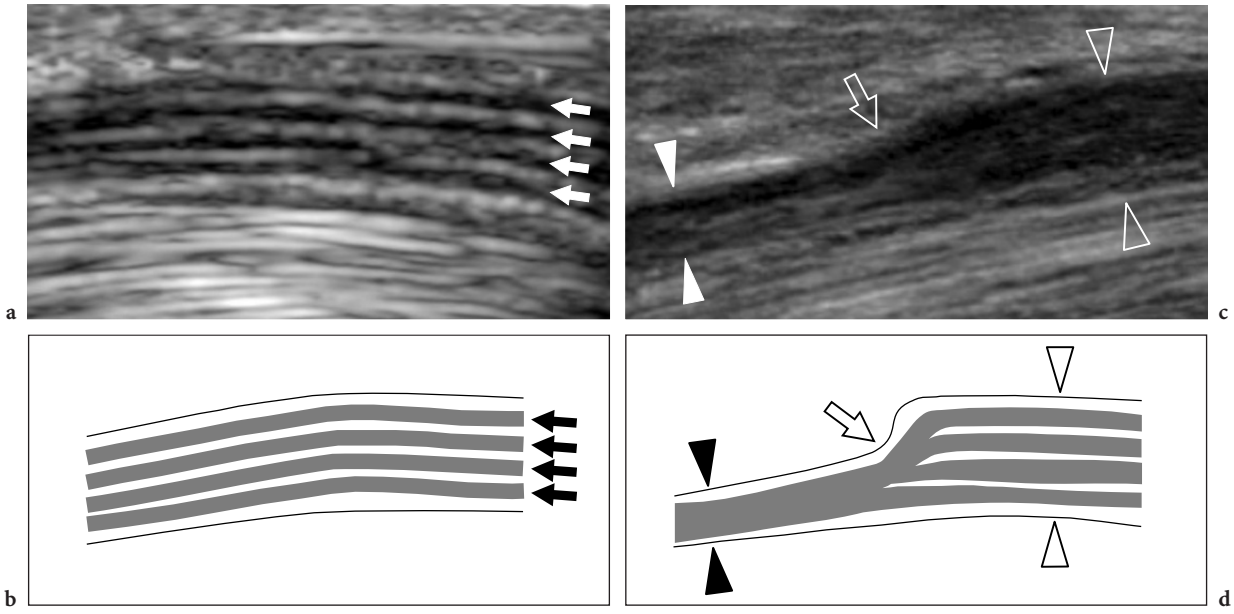

Fig. 4.8a–d. Entrapment neuropathies: nerve shape changes. **a** Long-axis 15–7 MHz US image of the median nerve at the carpal tunnel level with **b** schematic drawing correlation in a healthy volunteer demonstrates a normal-sized nerve and clear delineation of the fascicular arrangement (*arrows*). **c** Corresponding long-axis 17–5 MHz US image of the median nerve in a patient with severe median neuropathy reveals an abrupt change (*arrow*) in the size of the nerve at the proximal edge of the retinaculum (compression point). The nerve is flattened (*white arrowheads*) within the carpal tunnel and markedly swollen (*open arrowheads*) proximal to the level of compression

close proximity to the compression level, where the nerve abruptly flattens. Given these features, US is an accurate means of identifying the level of compression as located just ahead of the swollen nerve portion. Although nerve flattening should be regarded as the main sign of nerve compression, quantitative analysis of nerve thickening by means of the ellipse formula [(maximum AP diameter) × (maximum LL diameter) × (π/4)] has proved to be the most consistent criterion for the diagnosis at various entrapment sites (Chiou et al. 1998; Duncan et al. 1999; Bargfrede et al. 1999). As an ancillary finding, dynamic scanning may show a reduced mobility of the nerve over the mass or beneath the retinaculum, but this latter sign is too subjective and hard to quantify with US (Nakamichi and Tachibana 1995). At least at the carpal tunnel level, the cross-sectional area of the median nerve has also been regarded as an index for selecting patients with severe disease for which surgical decompression is indicated (Lee et al. 1999). It is conceivable that loss of axons may be associated with nerve enlargement as an expression of an increased amount of endoneural edema (Beekman et al. 2004b). In entrapment neuropathies, the nerve echotexture may become uniformly hypoechoic with loss of the fascicular pattern at the level of the compression site and proximal to it (Fig. 4.9). In general, the hypoechoic changes occur gradually and become more severe as the nerve nears the site of compression (Martinoli et al. 2000b). They derive from swelling of the individual fascicles and decreased echogenicity of the epineurium. The outer lining of the nerve, which is normally undefined and part of a continuum with the epineurium and surrounding fat, becomes sharp and well delineated. Depiction of such changes may increase confidence in the diagnosis and in determining the exact level of the lesion. In cases of entrapment by scar tissue, diagnostic difficulties may arise in distinguishing echotextural changes related to the compressed nerve from the scar itself, because of a similar hypoechoic appearance. Then, an enhanced depiction of intraneural blood flow signals can be appreciated with color and power Doppler techniques as a sign of local disturbances in the nerve microvasculature that occur in a compressive context (Martinoli et al. 2000b). The hypervascular pattern is more clearly appreciated in swollen hypoechoic nerves of patients with chronic, longstanding disease. Intranervous flow signals are made up of many vessel pedicles that enter the nerve from the superficial epineurium to run perpendicular to the fascicles (Fig. 4.10) (Martinoli et al. 1999, 2000b).

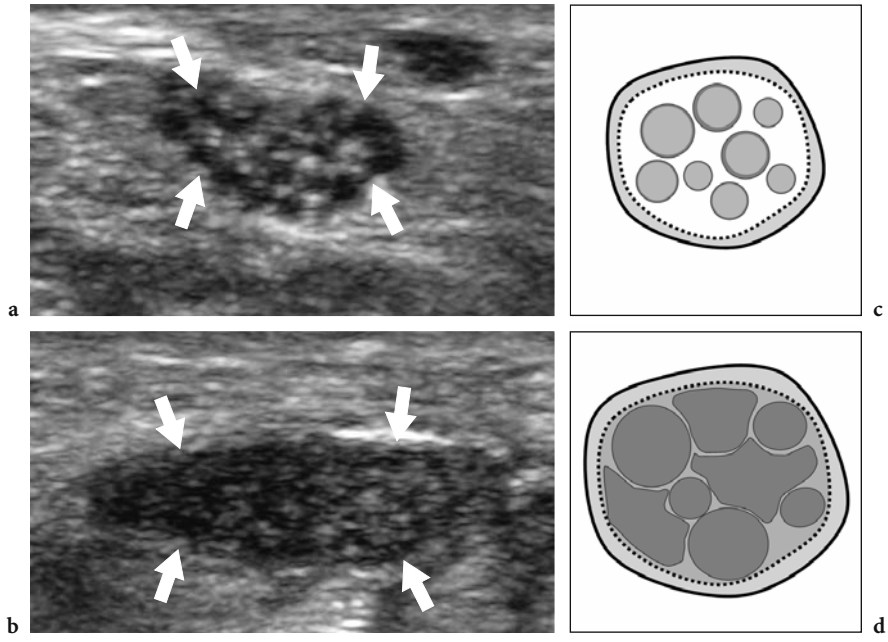

Fig. 4.9a–d. Entrapment neuropathies: echotextural changes. **a,b** Short-axis 17–5 MHz US images of the right median nerve obtained **a** at the distal radius and **b** just ahead of the compression point in a patient with longstanding carpal tunnel syndrome. As the nerve (*arrows*) approaches the site of compression, increasing hypoechoic changes are detected due to crowding of edematous fascicles and reduced echogenicity of the epineurium. This leads to a complete loss of the fascicular echotexture. **c,d** Schematic drawing correlation

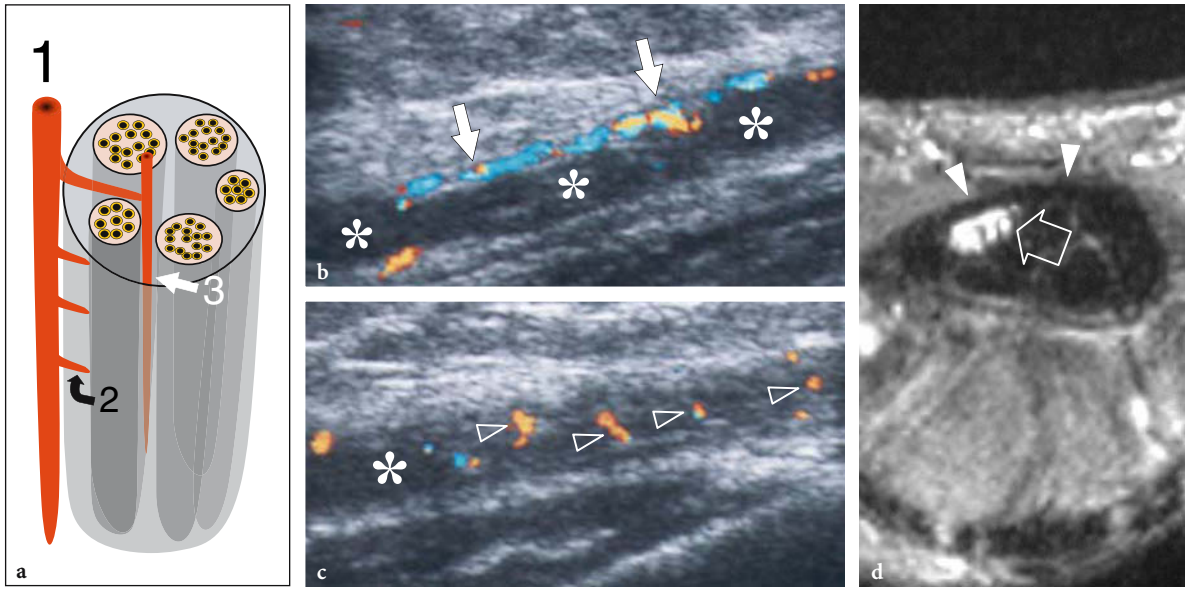

Fig. 4.10a–d. Entrapment neuropathies: microvascular changes. **a** Schematic drawing illustrates the nerve vascular system, made up of perineural vessels (*1*) coursing alongside the nerve. These vessels give off intraneural branches that pierce the outer epineurium (*2*) and distribute longitudinally (*3*) among the fascicles. **b,c** Long-axis 12–5 MHz color Doppler US images of the median nerve (*asterisks*) in a 56-year-old patient with carpal tunnel syndrome demonstrate subtle flow signals from the longitudinal perineural plexus (*arrows*) and a series of intranervous branches (*arrowheads*) running among the fascicles. **d** Corresponding transverse Gd-enhanced fat-suppressed T1-weighted MR image obtained just deep to the flexor retinaculum (*arrowheads*) reveals marked uptake of contrast material in the median nerve (*arrow*)

Based on the US assessment, nerve entrapment syndromes can be divided into three main classes. The first includes large nerves (i.e., the median, the ulnar, the radial, the sciatic, the tibial, etc.) which are easily depicted with US at the site of compression. In these cases, US evaluation can be effectively performed with conventional (mid-range) equipment and the diagnosis is based on pattern recognition analysis and quantitative measurements. The second includes small nerves (i.e., the posterior and anterior interosseous, the musculocutaneous, the peroneal, the sural, the plantars, etc.) the depiction of which requires high-end equipment and high-performance transducers. In these cases, quantitative measurements are usually not applied. The third class includes nerves which are not detectable with US because they are either too small (i.e., most part of the saphenous, etc.), or have too deep a course and are hidden by intervening bone (i.e., the suprascapular nerve, the intrapelvic course of the sciatic and the femoral nerve, etc.). In these cases, the US diagnosis is based only on the indirect evaluation of the innervated muscles to identify denervation signs (see Chapter 3). In the first two classes, there are many sites of nerve entrapment that are amenable to US examination in the upper and lower limb, and whatever the site and the nerve involved, the US signs described previously are virtually pathognomonic of compressive neuropathy. They include: the spinoglenoid-supraspinous notch area in the posterior shoulder for the suprascapular nerve (see Chapter 6) (Martinoli et al. 2003); the quadrilateral space for the axillary nerve (see Chapter 6) (Martinoli et al. 2003; the spiral groove of the humerus for the radial nerve (see Chapter 7) (Peer et al. 2001; Bodner et al. 1999, 2001; Rossey-Marec et al. 2004; Martinoli et al. 2004); the supinator area at the elbow for the posterior interosseous nerve (see Chapter 8) (Bodner et al. 2002b; Chien et al. 2003; Martinoli et al. 2004) and the wrist for the superficial branch of the radial nerve (see Chapter 10); the cubital and Guyon tunnels for the ulnar nerve (see Chapters 8, 10) (Chiou et al. 1998; Puig et al. 1999; Okamoto et al. 2000; Martinoli et al. 2000b, 2004; Nakamichi et al. 2000; Bianchi et al. 2004; Beekman et al. 2004a; Beekman and Visser 2004); the middle forearm for the anterior interosseous nerve (see Chapter 9) (Hide et al. 1999) and the carpal tunnel for the median nerve (see Chapter 10) (Altinok et al. 2004; Buchberger et al. 1991, 1992; Nakamichi and Tachibana 1995; Bertolotto et al. 1996; Lee et al. 1999; Chen et al.

1997; Duncan et al. 1999; Martinoli et al. 2002b; Kele et al. 2003; Bianchi et al. 2004; El Miedany et al. 2004; Yesildag et al. 2004; Wilson 2004; Wong et al. 2004; Kotevoglu and Gülbahce-Saglam 2005; Koyuncuoglu et al. 2005; Ziswiler et al. 2005); the posterior hip or proximal thigh for the sciatic nerve (see Chapter 12) (Graif et al. 1991); the fibular head and neck for the common peroneal nerve (see Chapter 14) (Martinoli et al. 2000b); the tarsal tunnel for the tibial nerve (see Chapter 16) (Martinoli et al. 2000b) and the intermetatarsal spaces for the interdigital nerves (see Chapter 17) (Redd et al. 1989; Read et al. 1999; Sobiesk et al. 1997; Quinn et al. 2001). A detailed overview of these syndromes is reported later in the chapters on the individual anatomic sites.

With respect to the electrophysiologic findings, a positive correlation between the nerve cross-sectional area and the severity of electromyographic findings has been found, whereas only a modest negative correlation seems to exist between electrodiagnostic parameters, such as motor velocity, CMAP amplitude, distal SNAP, and the nerve cross-sectional area (Kele et al. 2003; Beekman et al. 2004; El Miedany et al. 2004; Ziswiler et al. 2005). Generally speaking, US can complement nerve conduction studies in the evaluation of nerve entrapment syndromes. It can be informative in patients with absent motor or sensory responses, when it is difficult to localize the site of compression. A positive US study can reduce the uncertainty of nerve conduction studies and, therefore, reduces the need for further exclusionary studies. In addition, US can identify abnormal findings in the nerve surroundings, such as synovitis, space-occupying masses, or anomalous muscles, providing important information in the preoperative setting.

After surgical decompression, the US appearance and mobility of the affected nerves may improve, and it is possible to visualize the altered morphology of the osteofibrous tunnel after release of the retinaculum (Martinoli et al. 2000b; El-Karabaty et al. 2005).

4.1.6 Traumatic Injuries

Traumatic nerve injuries derive from traction, contusion, and penetrating trauma. Here we attempt a brief overview of nerve trauma according to the different mechanisms involved. In many cases, however, multiple mechanisms may coexist and, therefore, an exact differentiation among them is not always feasible in clinical practice.

4.1.6.1 Stretching Injuries

Nerve stretching injuries typically occur as a result of repetitive sprain or strain lesions, as well as with overuse. A characteristic injury is the avulsion of the nerve roots that occurs in brachial plexus trauma during motor vehicle accidents (see Chapter 6) (Shafighi et al. 2003; Graif et al. 2004). Another typical site of nerve traction is the popliteal fossa, where the peroneal nerve may be stretched during high-grade sprains, knee dislocation or fractures (see Chapter 12) (Gruber et al. 2005). In complete nerve lacerations, US reveals disruption of the fascicles with retraction and a wavy course of the nerve ends (Shafighi et al. 2003; Graif et al. 2004; Gruber et al. 2005). The outer nerve sheath may be intact. If traction injury causes partial nerve tear, a spindle neuroma (traction neuroma) can develop as an irregular swelling of hypoechoic tissue along the course of the severed nerve without evidence of nerve discontinuity (Fig. 4.11; see also Chapters 6, 12) (Bodner et al. 2001; Graif et al. 2004). In mild cases, the neuroma may involve only one or a few fascicles while the cross-sectional area of the nerve appears fairly normal or slightly enlarged.

4.1.6.2 Contusion Trauma

Contusion trauma most often occurs where nerves run closely apposed to bony surfaces at sites of low mobility and, are therefore, more vulnerable to external injuries. In most cases, such trauma is self-resolving and does not cause morphologic changes detectable with US (Fig. 4.12). Repeated minor contusion trauma is usually required to cause abnormalities within the nerve substance that can be detected with US. A typical contusion trauma is that involving the radial nerve where it pierces the lateral intermuscular septum, or the deep peroneal nerve against the midfoot bones in soccer players who receive repeated blows over the dorsum of the foot (see Chapter 17) (Schon 1994; Quinn et al. 2001). These lesions lead to development of a segmental fusiform thickening of the nerve at the site of trauma. A peculiar kind of contusion trauma is that involving unstable ulnar nerves at the cubital tunnel in patients with absence of the Osborne retinaculum. In predisposed subjects, the repeated friction of the nerve against the epicondyle during elbow flexion may cause chronic damage and functional deficit, so-called "friction neuritis". In these cases, the nerve appears swollen and hypoechoic as a result

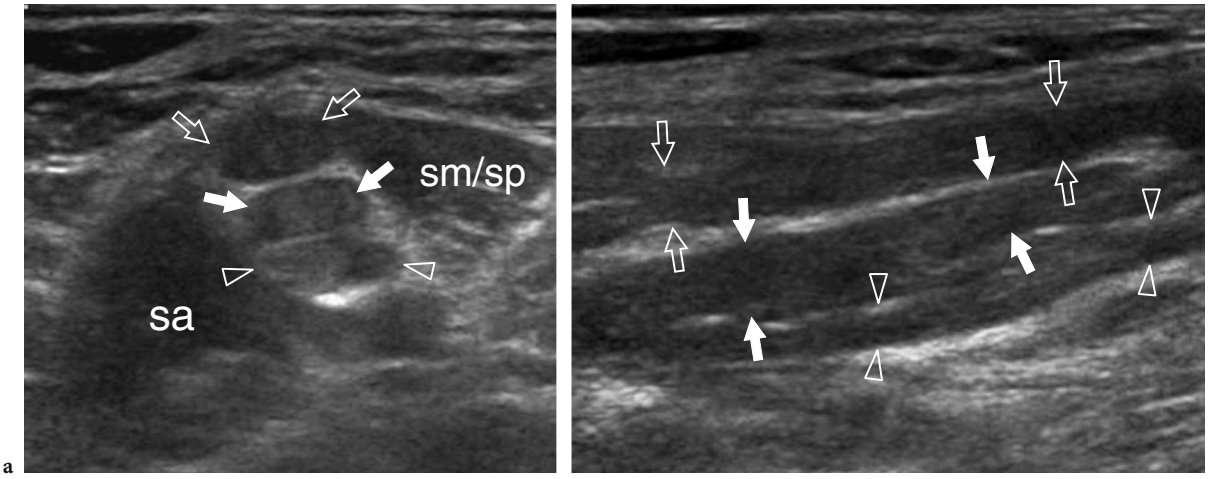

Fig. 4.11a,b. Stretching injury (burner/stinger syndrome) of the brachial plexus nerves in a 25-year-old rugby player with persistent tingling radiating from the left shoulder to the hand and progressive weakness of the limb muscles after a significant contact injury. **a** Short-axis and **b** long-axis 12–5 MHz US images over the interscalene area demonstrate segmental thickening of the C5 (*open arrows*), C6 (*white arrows*), and C7 (*arrowheads*) components of the plexus (upper and middle trunks), reflecting fusiform neuromas related to stretching trauma. *sa*, scalenus anterior; *sm/sp*, scalenus medius/scalenus posterior muscles. In the burner/stinger syndrome, MR imaging of the cervical spine should always be performed to rule out nerve damage inside the spinal canal as well as herniated disks, ligament injuries, facet injuries, and undisplaced fractures

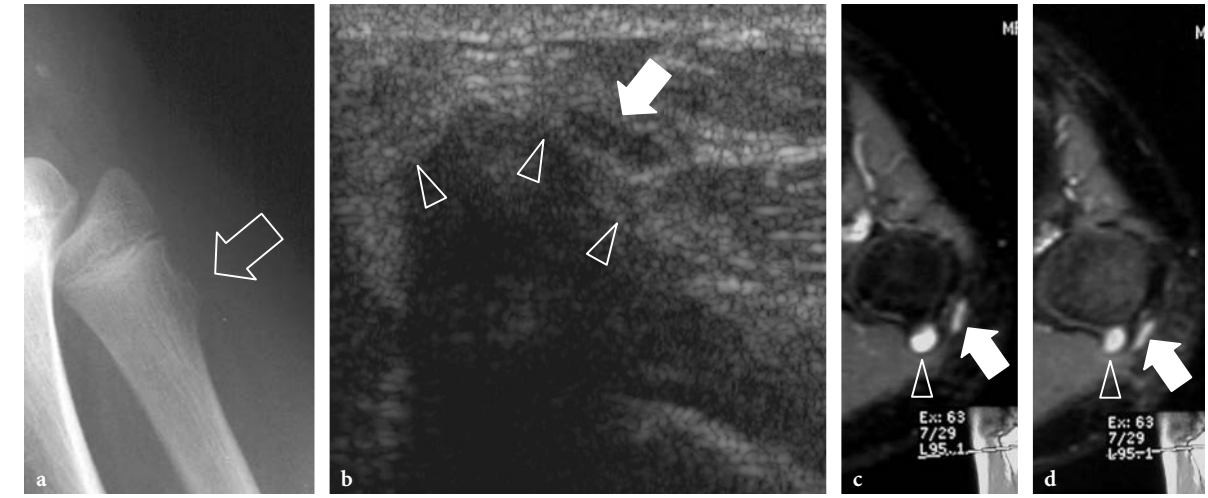

Fig. 4.12a–d. Nerve contusion trauma. Peroneal neuropathy in a 15-year-old boy with onset of foot-drop after receiving a blow on the lateral knee. **a** Lateral plain film demonstrates an exostosis (*arrow*) at the fibular metaphysis. **b** Transverse 12–5 MHz US image reveals impingement of the peroneal nerve (*arrow*) against the cartilaginous component (*arrowheads*) of the exostosis. The nerve is swollen and hypoechoic. **c,d** Correlative transverse fat-suppressed GRE T2* MR images demonstrate a hyperintense nerve (*arrow*) crossing the exostosis (*arrowhead*). Note the T2-hyerintense cap of the exostosis

of fibrotic changes and shows a thickened external epineurium (see Chapter 8) (Jacobson et al. 2001).

4.1.6.3 Penetrating Wounds

In penetrating wounds (glass fragments are often involved!), there may be a partial or complete interruption of the nerve fascicles. Regenerating Schwann cells and axons grow randomly at the lesion site in an attempt to restore the continuity of the nerve. Generally, the gap between the separated fascicles is wide, and new axonal sprouts develop in many directions. A hypoechoic fibrous mass is the result of such a disorganized repair process. In complete tears, stump neuromas (terminal neuromas) appear as small hypoechoic masses in continuity

with the opposite edges of the severed nerve (see Chapters 9, 10) (Provost et al. 1997; Graif et al. 1991; Simonetti et al. 1999). Usually, their size is slightly larger than the axial diameter of the nerve. Most have well-defined margins; however, when they are attached to the surrounding tissues by adhesions and encasing scar tissue, their borders may be irregular or poorly defined (Bodner et al. 2001). US depiction of terminal neuromas may map the location of the nerve ends, which may be displaced and retracted from the site of the injury (Fig. 4.13a–c). When the nerve ends are close together, the bulk of neuroma may encase them mimicking a partial tear. In some way, this seems to suggest that US is unable to quantify the grade of nerve damage within a spindle neuroma. When the nerve is partially torn, the hypoechoic neuroma may encase resected and preserved fascicles giving rise to a homogeneous fusiform swelling of the nerve or can be seen arising specifically from the resected fascicles, while the unaffected fascicles can be appreciated continuing their course alongside the fibrous mass (Fig. 4.14). In this latter instance, US is able to estimate the amount (percentage) of fascicles involved in the neuroma (Fig. 4.14d). Overall, US may help the clinical examination and nerve conduction studies to provide information about the condition of the injured nerve, and especially in deciding whether early surgical treatment is required. This is particularly true for minor nerve lesions without axonal damage.

4.1.6.4 Postoperative Features

In patients with partial nerve tear, a delicate procedure of internal neurolysis of the nerve and its sheath is mainly used for either repairing the interrupted nerve fascicles or removing intraneural scar tissue. With this procedure, the main risk consists of inadvertent damage to preserved fascicles and formation of a new postoperative scar close to the nerve surface. With complete transection of the nerve, a more complex surgical procedure is required. The appropriate selection of an adequate reconstruction technique depends on the length of the gap intervening between the nerve ends after removal of irreversibly damaged tissue and terminal neuromas. Where the gap is short, an "end-to-end" anastomosis is preferred given that substantial tension on the sutured

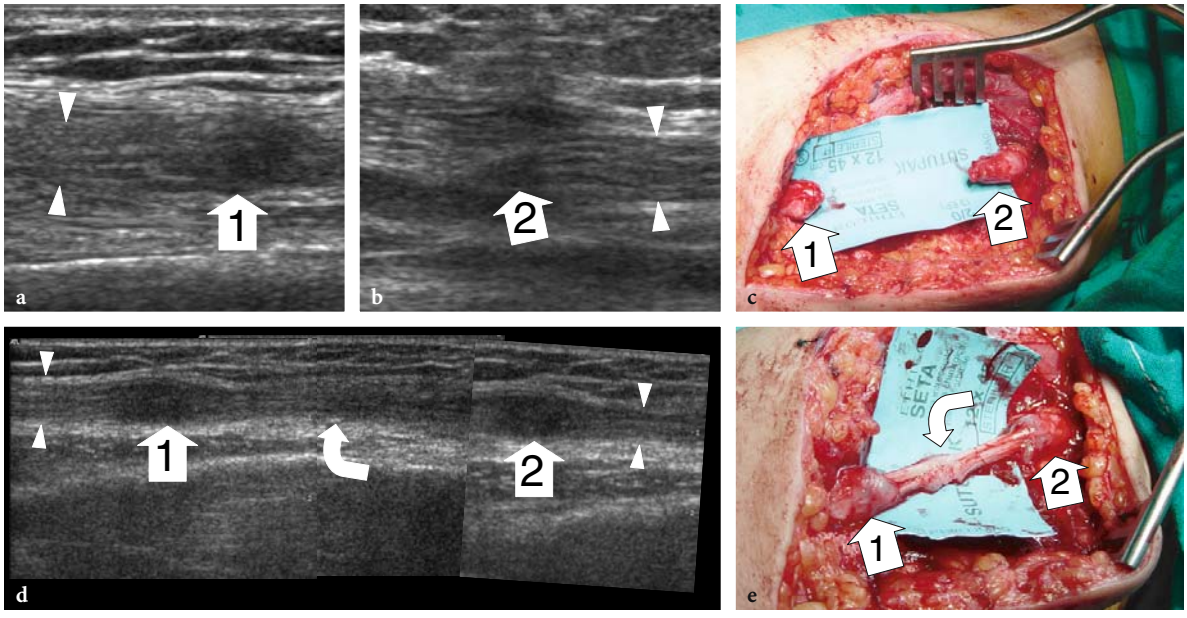

Fig. 4.13a–e. Complete nerve tear in a 12-year-old girl with loss of function of the median nerve after receiving a penetrating injury to the arm by a glass fragment. In the acute setting, the patient was operated on for laceration of the brachial artery. **a,b** Long-axis 15-7 MHz US images at the level of injury demonstrate discontinuity of the median nerve. Note the proximal and distal stumps (*arrowheads*) of the severed nerve ending in a hypoechoic terminal neuroma (*1*, *2*). **c** Gross surgical view shows discrete retraction (4 cm gap) of the nerve ends. **d** After reconstructive surgery, a long-axis 12–5 MHz US image demonstrates the sural nerve graft (*curved arrow*) interposed between the nerve ends (*arrowheads*). A fusiform hypoechoic thickening is observed at the proximal (*1*) and distal (*2*) site of anastomosis: it should be regarded as a normal finding. A split-screen image was used, with the two screens aligned for an extended field of view. **e** Surgical correlation

nerve stumps can be avoided. When the gap is wide, bridging with a nerve graft to obtain a "proximal nerve end–graft–distal nerve end" anastomosis is the technique of choice (Fig. 4.13d,e). For this latter procedure, tissue is usually harvested from minor superficial sensory nerves, such as the sural nerve or the medial brachial and antebrachial cutaneous nerves. Very thin sutures placed within the outer and interfascicular epineurium are used for the anastomosis. They are easily appreciated with US as bright hyperechoic spots within the nerve substance and should not be mistaken for pathologic findings, such as calcifications in granulomatous tissue (Fig. 4.15). In nerve reconstructive surgery, US allows a reliable postoperative evaluation of the continuity of nerve at the anastomosis, and can rule out perineural col-

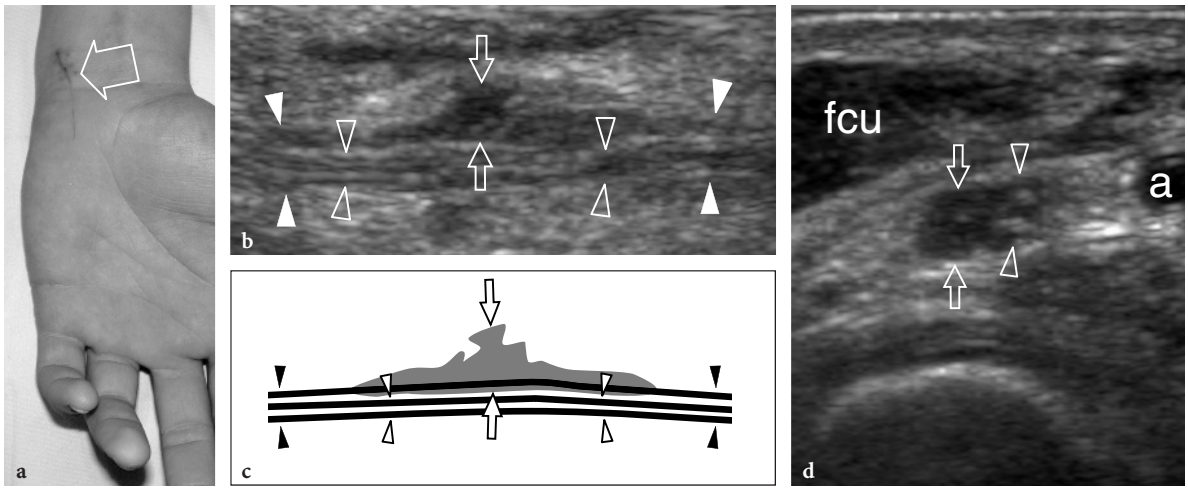

Fig. 4.14a–d. Partial-thickness tear of the ulnar nerve at wrist in a 15-year-old boy. The wound was produced by a sharp object and resulted in a selective motor deficit. **a** Photograph shows the site of injury (*arrow*). Observe the semiflexion deformity of the ring and little fingers related to weakness of ulnar-innervated interosseous muscles. **b** Long-axis 15–7 MHz US image over the main trunk of the ulnar nerve (*white arrowheads* in **b**, *black arrowheads* in *c*) with **c** schematic drawing correlation reveals hypoechoic tissue (*arrows*) involving part of the nerve fascicles, whereas some preserved fascicles (*open arrowheads*) are seen crossing the site of injury unaffected. **d** Short-axis 15–7 MHz US image demonstrates the affected (*arrows*) and preserved (*arrowheads*) portions of the ulnar nerve. Hypoechoic fibrous tissue is seen involving approximately 50% of the medial-sided fascicles of the nerve, those giving rise to the deep motor branch. Conversely, the normal lateral-sided fascicles will continue in the superficial sensory branch of the nerve. *a*, ulnar artery; *fcu*, flexor carpi ulnaris muscle

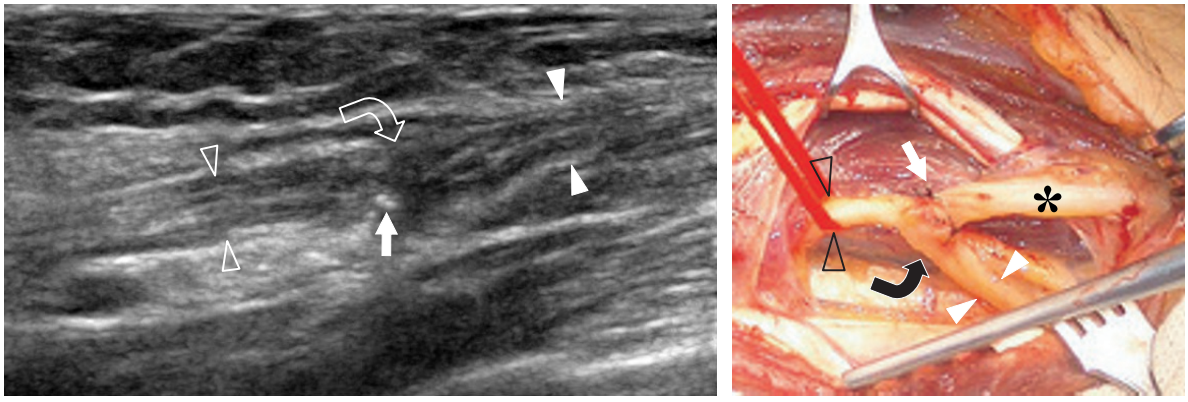

Fig. 4.15a,b. Nerve reconstructive surgery. This 62-year-old man underwent amputation of the median nerve at the forearm due to encasement by a soft-tissue sarcoma. While the proximal nerve stump was implanted in the flexor digitorum superficialis muscle, the distal stump was anastomosed with the ulnar nerve using a termino-lateral suture. After surgery, there was partial recovery of median nerve function. **a** Long-axis 17–5 MHz US image over the anastomosis with **b** correlative surgical view shows the distal stump of the median nerve (*white arrowheads*) sutured to the ulnar nerve (*open arrowheads*). Note a certain amount of spindle-shaped thickening of the nerve at the site of anastomosis (*curved arrow*) with some fine stitches (*straight arrow*) appearing as tiny hyperechoic dot-like structures at the surface of the nerve. *Asterisk*, ulnar nerve distal to the anastomosis

lections. A mild and fusiform increase in the nerve size at the sutures level is a normal finding. In contrast, marked irregular bulging of hypoechoic tissue at the anastomosis, possibly involving one side of the nerve, should be regarded as a pathologic sign, indicating inadequate fusion of the nerve edges and postsurgical neuroma formation (Graif et al. 1991; Peer et al. 2001). Excessive tension on the nerve edges and infection are possible causes of defective anastomosis. In this clinical setting, US may compensate for the limitations of electrodiagnosis and clinical examination by yielding reliable information on the size, extent, and localization of postsurgical scarring and neuromas with respect to further surgical intervention (Peer et al. 2003).

In addition to primary (trauma-related, neurolysis-related) causes, scar formation may occur following surgery that has not been primarily directed to the nerve (i.e., fracture repair, vascular surgery, etc.). Scar tissue may encase the nerve as a whole or may lie adherent to its surface (Fig. 4.16). The nerve appears flattened and indistinguishable within the scar or may be distorted at its periphery with reactive focal swelling related to edema and venous congestion (Fig. 4.16c,h). Under these circumstances, nerve scarring may lead to persistent pain and delayed recovery of nerve function because of constant traction on the nerve and limited capability for longitudinal translation during joint movements. In the postoperative setting, US findings of incidental iatrogenic injuries to peripheral nerves have been reported in the radial, femoral, accessory, and sciatic nerves (Graif et al. 1991; Peer et al. 2001; Bodner et al. 2002a; Gruber et al. 2003).

4.1.7 Rheumatologic and Infectious Disorders

In several rheumatologic disorders, such as rheumatoid arthritis, polyarteritis nodosa, Wegener's granulomatosis, and Churg-Strauss and Sjögren syndromes, one of the clinical landmarks of vasculitis is the appearance of neurologic findings (Lanzillo et al. 1998; Rosenbaum 2001). From the pathophysiologic point of view, vasculitis-related neuropathy affects large nerve trunks producing a multifocal degeneration of fibers as a result of necrotizing angiopathy of small nerve arteries, so-called multiple mononeuropathy (Said and Lacroix 2005). In these patients, the neuropathy does not correlate with disease parameters, such as disease activity, rheumatoid factor, and functional and radiologic scores, and there is sequential involvement of individual nerves both in time and anatomically (Nadkar et al. 2001). Nerve conduction velocities are usually not markedly reduced from normal, provided that the compound nerve or muscle action potential is not severely reduced in amplitude (Sivri and Guler-Uysal 1998). Although multiple mononeuropathy is the most common manifestation, nerve entrapment syndromes may also occur at sites where nerves pass in close proximity to either a synovial joint (i.e., cubital tunnel, tarsal tunnel, Guyon tunnel) or one or more synovial-sheathed tendons (i.e., flexor tendons at the carpal tunnel, flexor hallucis longus at the tarsal tunnel) or para-articular bursae (i.e., iliopsoas bursa at the hip). Because the clinical evaluation of nerves is often limited in these patients by simultaneous symptoms resulting from joint involvement, US imaging can contribute to distinguishing entrapment neuropathies related to derangement of joints, effusions, and synovial pannus from non-entrapment neuropathy. This is based on the fact that multiple mononeuropathy does not lead to an altered morphology of the affected nerve, whereas entrapment neuropathies do.

4.1.7.1 Leprosy

Leprosy (Hansen disease) is a chronic infectious disease caused by *Mycobacterium leprae*, which, in its many and various clinical forms, involves the skin and nerves (Fig. 4.17a). Although in the Western world leprosy is almost only seen in immigrants, it is endemic in developing countries (tropics and subtropics) with 12 million people affected; it therefore represents the most diffuse neuropathy in the world. Leprosy is probably spread by droplet infection, but prolonged household contact is needed and most people are not susceptible to the disease. From the clinical point of view, leprosy can be grouped into two polar forms – tuberculoid and lepromatous – between which borderline forms show an intermediate spectrum of phenotypes (Ridley and Jopling 1966). In tuberculoid leprosy, there is an intense immune response: aggressive infiltration of epithelioid and lymphoid cells into the nerve causes thickening of the epineurium and perineurium and destruction of fascicles. In the lepromatous type, the immune response is indolent and active proliferation of bacilli occurs: this form shows better preservation of the nerve architecture. Transition

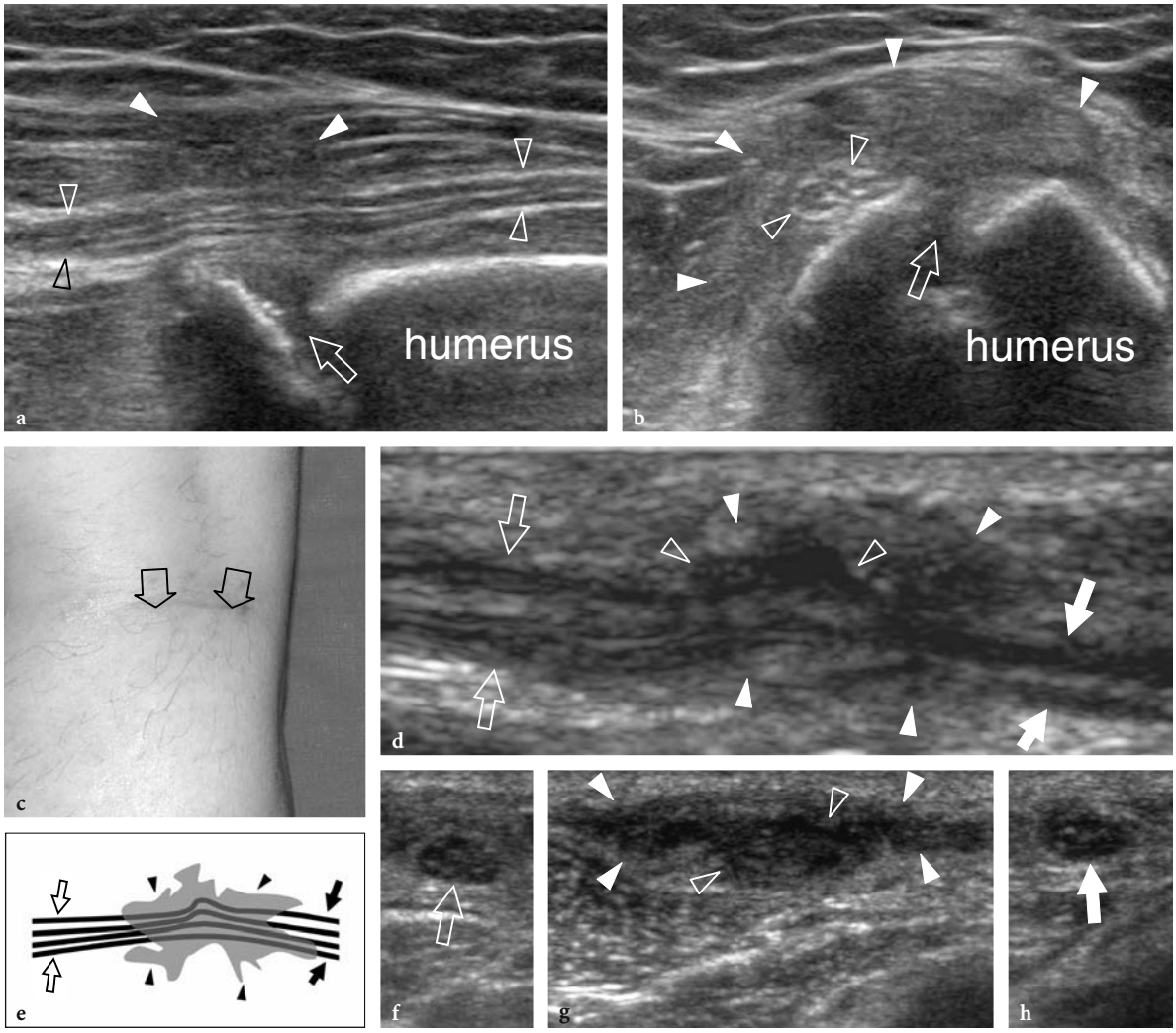

Fig. 4.16a–h. Postoperative encasement of nerves by scar tissue. Two different cases. **a,b** Radial nerve buried in a fibrous callus after repair of humeral shaft fracture. **a** Long-axis and **b** short-axis 17–5 MHz US images show focal encasement of the radial nerve (*open arrowheads*) by an ill-defined hypoechoic mass (*white arrowheads*) developing over the fracture site (*arrow*) reflecting the formation of fibrous callus. The nerve's fascicular echotexture is retained within the callus. The patient underwent a second surgical look to free the nerve from the callus. **c–h** Peroneal nerve encased in a scar after surgical stripping of the saphenous vein. **c** Photograph shows the surgical access. **d** Long-axis 12–5 MHz US image of the peroneal nerve (*arrows*) with **e** schematic drawing correlation reveals distortion and pinching of the nerve fascicles (*open arrowheads*) by hypoechoic scar tissue (*white arrowheads*). **f–h** Short-axis 12–5 MHz US images obtained from **f** proximal to **h** distal show the normal peroneal nerve (*open arrow*) which becomes indistinguishable (*open arrowheads*) within the scar (*white arrowheads*) and then as it (*white arrow*) exits the scar to return to a normal appearance

toward a higher resistance form of leprosy may produce episodes of acute neuritis, such as the so-called "reversal reaction" and "erythema nodosum leprosum". During these phases, a nerve segment may become intensely painful and tender. As the disease progresses, subsequent episodes of neuritis add to the deficit until the affected nerve may be completely destroyed. Sensory abnormalities usually precede paralysis. The initial symptom of nerve involvement is sensory loss, which increases the frequency of minor trauma, leading to infections and eventually to mutilating injuries, and blindness. The preferred sites of nerve swelling in leprosy are similar to those of entrapment neuropathies (i.e., the cubital tunnel for the ulnar nerve, the carpal tunnel for the median nerve, the fibular neck for

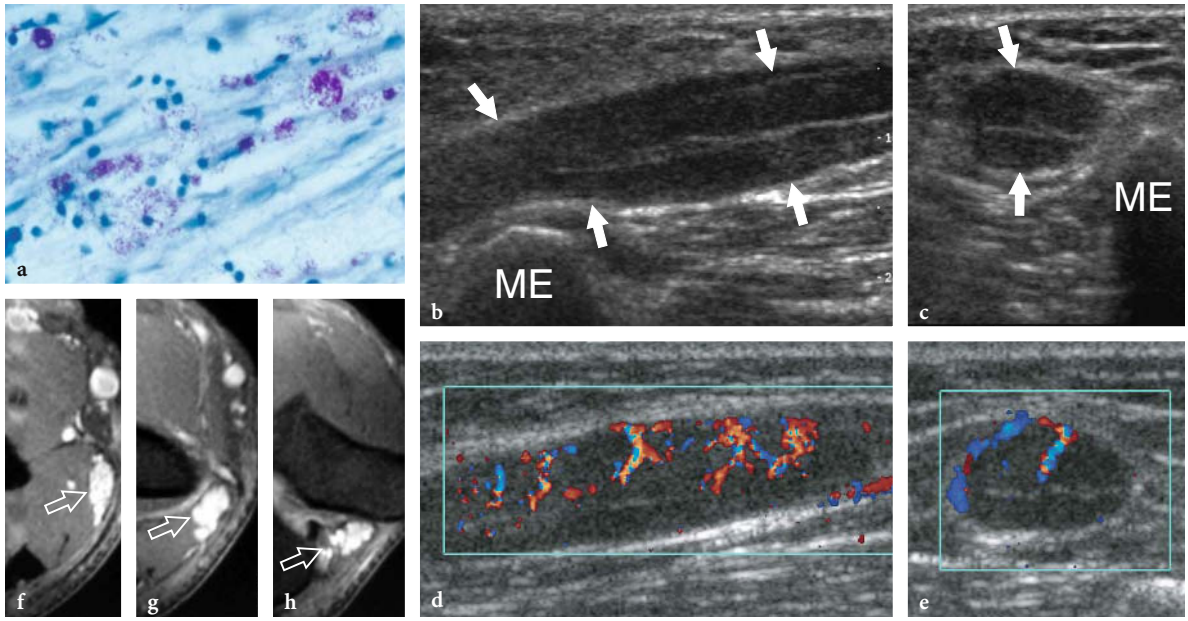

Fig. 4.17a–h. Reversal reaction in leprosy. **a** Microscopic view of the sural nerve in a 25-year-old patient with leprosy reveals the presence of *Mycobacteria* (*purple*) among the nerve tissue. Ziehl-Nielsen staining; original magnification ×800. **b–h** Right ulnar nerve of a 22-year-old man with borderline tuberculoid leprosy examined at the elbow during the course of a reversal reaction. **b** Long-axis and **c** short-axis gray-scale 12–5 MHz US images demonstrate high-grade swelling of the nerve (*arrows*) with smooth fusiform enlargement of individual fascicles. *ME*, medial epicondyle. Corresponding **d** long-axis and **e** short-axis color Doppler 12–5 MHz US images show dramatically increased blood flow within endoneural vessels. **f–h** Cranial to caudal sequence of Gd-enhanced fat-suppressed MR images through the medial elbow show marked contrast enhancement into the nerve (*arrow*)

the common peroneal nerve, the tarsal tunnel for the tibial nerve). Compared with a chronically compressed nerve, however, the nerve enlargement is more extensive and less circumscribed. In leprosy patients, US is able to reveal nerve abnormalities including nerve swelling, hypoechoic changes in the epineurium, and loss of the fascicular echotexture (Fig. 4.17b,c) (Martinoli et al. 2000c). These changes require multiple episodes of lepromatous reactions and a cumulative effect with time to become apparent at US. In fact, nerve enlargement correlates well with patients who previously underwent reversal reactions (Martinoli et al. 2000c). During the course of a reversal reaction, the affected nerve segment is markedly thickened, intensely painful and tender (Fornage and Nerot 1987; Martinoli et al. 2000c). The onset of these reactions can be indicated by an intraneural hyperemic pattern at color and power Doppler imaging (Fig. 4.17d-h) (Martinoli et al. 2000c). These signs suggest rapid progression of nerve damage and a poor prognosis unless antireaction treatment is started (Martinoli et al. 2000c). More rarely, "cold" soft-tissue abscesses may be seen arising from the affected nerve and spreading through the fascial planes of the limbs and extremities (Fig. 4.18).

4.1.8 Tumors and Tumor-Like Conditions

Peripheral nerve tumors include two main benign forms – the schwannoma (also referred to as neurinoma or neurilemmoma) and the neurofibroma – and the malignant peripheral nerve sheath tumor, which most often derives from the malignant (sarcomatous) transformation of a neurofibroma (Murphey et al. 1999). In addition, other masses, such as hemangiomas, lymphomas, and ganglion cysts, may occasionally develop within the nerve dissecting the fascicles and expanding inside the neural tissue. The occurrence of these masses is rare but they may cause nerve dysfunction and local symptoms and should not be mistaken for the more common nerve sheath tumors. Finally, a variety of extrinsic soft-tissue neoplasms, both benign with aggressive behavior and malignant, may involve a nerve during their local spread.

4.1.8.1 Peripheral Nerve Sheath Tumors

Peripheral nerve sheath tumors derive from Schwann cells. Pain and neurologic symptoms are unusual except in large tumors (Murphey et al. 1999; Reynolds et al. 2004). Generally speaking, the US diagnosis of these tumors is based on depiction of a solid hypoechoic mass in direct continuity with a nerve at its proximal and distal poles (Fornage 1988; Beggs 1999; Martinoli et al. 2000a; Lin and Martel 2001; Reynolds et al. 2004). Detection of the junction between the tumor and the nerve of origin requires careful scanning because the nerve ends may be distorted and stretched over the mass. In addition, the nerve origin of a mass arising from a small nerve (consisting of a single hypoechoic fascicle) may not be reliably assessed: this can be especially true in superficially seated lesions. Some differential features have been described among tumor histotypes, and especially between schwannomas and neurofibromas.

Schwannomas are slowly growing encapsulated tumors that are found more commonly in the extremities. They are composed of neoplastic cells that have the ultrastructural characteristics and antigenic phenotype of Schwann cells but do not contain axons (Woodruff 1993). Most appear as solitary globoid masses located along a nerve and eccentric to the nerve axis, with homogeneously hypoechoic echotexture, posterior acoustic enhancement, and a hypervascular pattern at color and power Doppler imaging (Fig. 4.19a,b) (Fornage 1988; Beggs 1999; Martinoli et al. 2000a; Lin and Martel 2001; Reynolds et al. 2004). Occasionally, intratumoral cystic changes related to accumulation of myxoid matrix (cystic schwannoma) and calcifications (ancient schwannoma) can be recognized (Fig. 4.20) (Isobe et al. 2004). Distinguishing cystic schwannomas from intraneural ganglia may be aided by the characteristic location of the latter (see below). In schwannomas, the proximal nerve end outside the tumor may appear thickened and hypoechoic with loss of the fascicular pattern, thus producing a tapering appearance to the oval mass. This can be appreciated even for a long nerve segment and seems, at least in part, to reflect the infiltration of tumor cells along the fascicles (Graif M.,

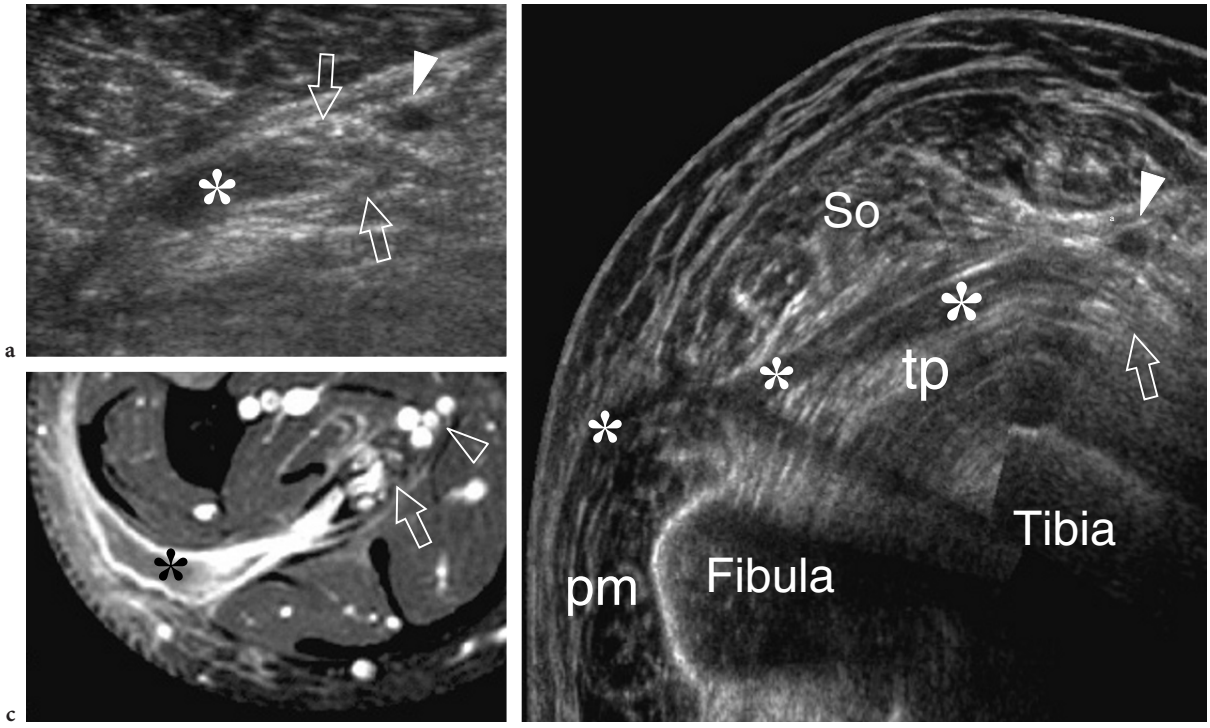

Fig. 4.18a–c. Neurogenic abscess in leprosy. **a** Transverse scan and **b** extended-field-of-view 12–5MHz US images over the tibial nerve (*arrows*) at the mid-distal third of the leg demonstrate a fluid collection (*asterisk*) arising from the nerve substance and spreading along the fascial planes, deep to the soleus muscle (*So*) and superficial to the tibialis posterior (*tp*) and the peroneals (*pm*). **c** Correlative Gd-enhanced fat-suppressed MR image shows discrete contrast enhancement in the abscess walls. Note the origin of the abscess from the nerve. *Arrowhead*, posterior tibial vessels. Aspiration of fluid revealed aseptic necrotic material

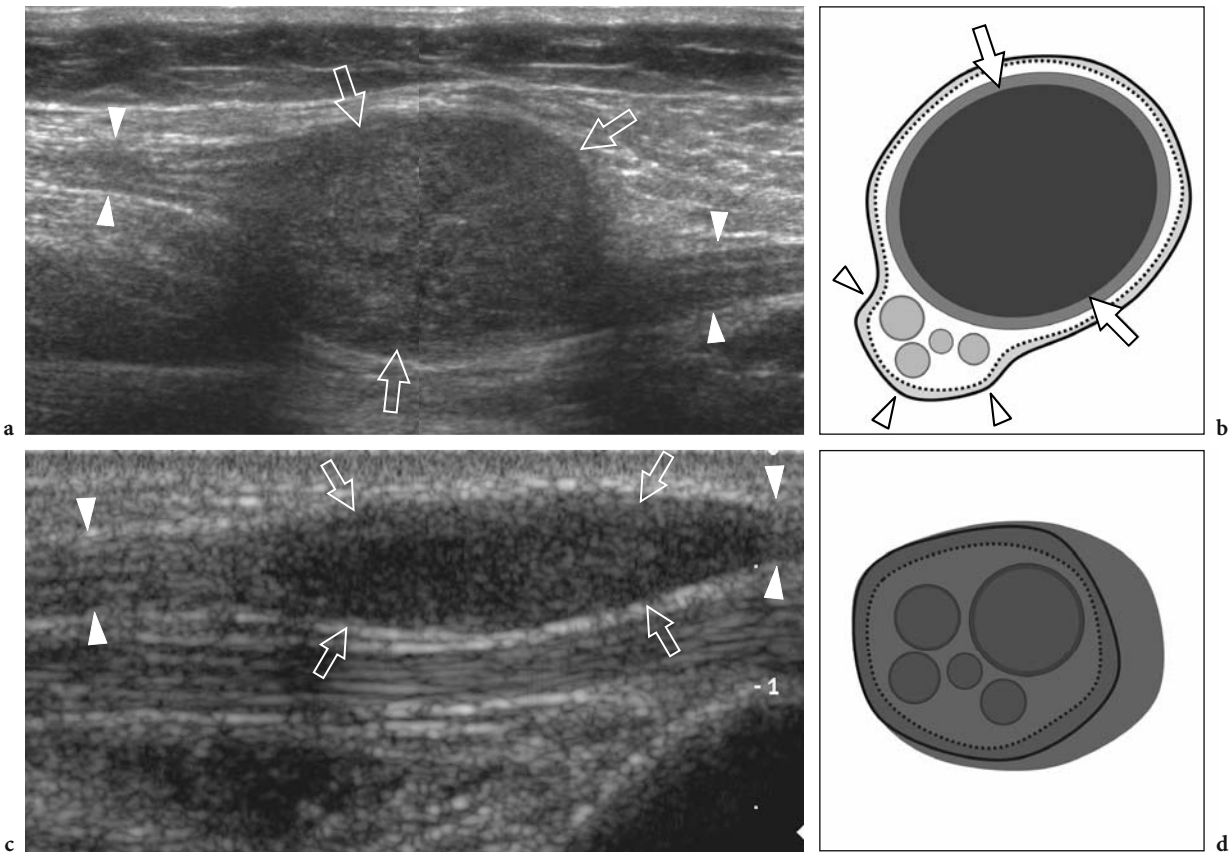

Fig. 4.19a–d. Peripheral nerve sheath tumors. **a,b** Schwannoma of the tibial nerve at the posterior leg. **a** Long-axis gray-scale 12–5 MHz US image with **b** schematic drawing correlation depicts the tumor as a globoid hypoechoic mass (*arrows*) which develops eccentrically at the periphery of the nerve (*arrowheads*). **c,d** Neurofibroma of the median nerve at the distal forearm. **c** Long-axis gray-scale 12-5 MHz US image with **d** schematic drawing correlation shows the tumor as a hypoechoic spindle-shaped mass (*arrows*) expanding within the nerve and involving the fascicles (*arrowheads*). Focal enlargement of the nerve and disappearance of the fascicular pattern is observed

unpublished data). Such abnormalities are usually not seen in the distal end of the affected nerve. In addition, schwannomas may be seen developing from an individual fascicle, which appears diffusely thickened even at a distance from the mass, whereas the other fibers of the same nerve are displaced by the bulk of the tumor but remain unaffected with regard to size and echotexture (Fig. 4.21a). This can explain why some schwannomas seems to have central continuity with the long axis of the nerve.

Neurofibromas, on the other hand, are intimately associated with the parent nerve, developing in a fusiform (not globoid) fashion, with the nerve entering and exiting from the extremities of the lesion (Fig. 4.19c,d) (King et al. 1997; Lin and Martel 2001). Histopathologically, they are composed of a mixture of cell types, the predominant one of which has characteristics of the perineurial cells. As the proliferative cells of a neurofibroma grow, they spread through the epineurium into the surrounding soft tissue. Neurofibromas can be categorized into three forms: localized, diffuse, and plexiform (associated with type 1 neurofibromatosis). The localized variety is the most common, accounting for approximately 90% of cases (Murphey et al. 1999). Often, a target sign formed by a subtle central hyperechoic region within the hypoechoic mass can be found in these tumors, reflecting a central fibrotic focus surrounded by peripheral myxomatous tissue (Fig. 4.21b–d) (Lin et al. 1999). Neurofibromas are less hypervascular than schwannomas at color and power Doppler imaging. Unlike localized neurofibromas, diffuse neurofibromas primarily involve the skin and the subcutaneous tissue and presents as a plaque-like elevation of the skin with thickening of the subcutaneous tissue (Fig. 4.22a,b) (Murphey et al. 1999).

As regards the malignant peripheral nerve sheath tumor, the only findings which may make the exam-

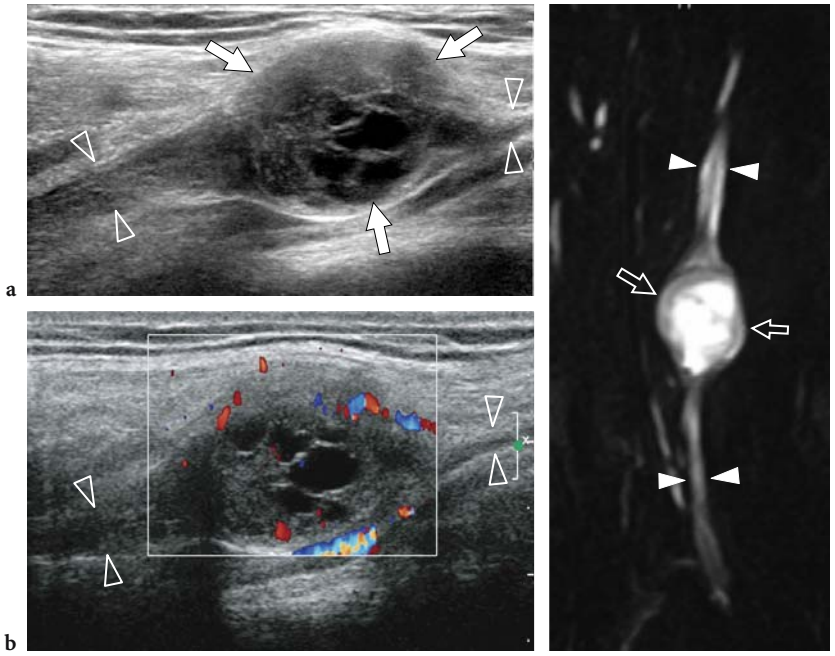

Fig. 4.20a–c. Cystic schwannoma. **a,b** Long-axis **a** gray-scale and **b** color Doppler 12–5 MHz US images over the radial nerve (*arrowheads*) at the arm with **c** MR-neurographic correlation show a rounded mass (*arrows*) with intratumoral cystic changes, related to accumulation of myxoid matrix, in continuity with the parent nerve (*arrowheads*). The tumor exhibits a hypervascular pattern made up of peripheral and central color Doppler signals

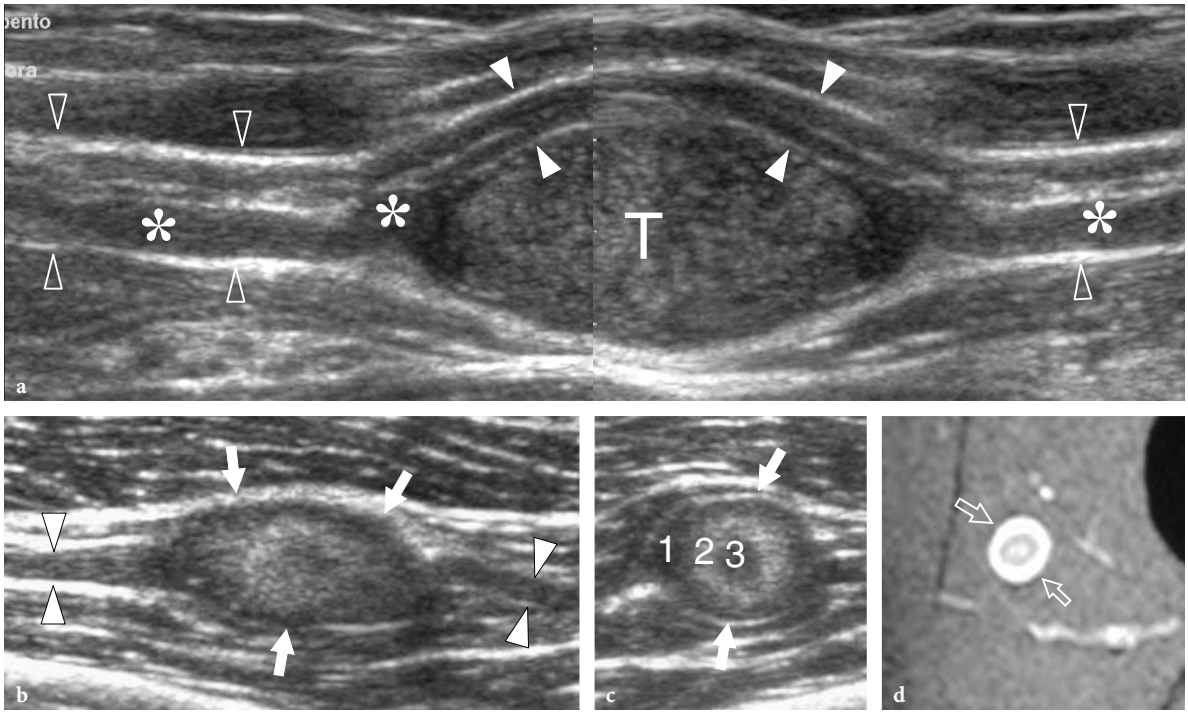

Fig. 4.21a–d. Peripheral nerve sheath tumors: peculiar US findings. Two different cases. **a** Schwannoma of the median nerve at the bicipital sulcus. Long-axis 12–5 MHz US image depicts the tumor (*T*) as an eccentric hypoechoic mass in continuity with the nerve (*open arrowheads*). At its proximal and distal ends, the tumor is connected with a swollen fascicle (*asterisks*), whereas the other fascicles (*white arrowheads*) remain unaffected and displaced at the periphery of the mass. A split-screen image was used, with the two screens aligned for an extended field of view. **b–d** Neurofibroma. **b** Long-axis and **c** short-axis 12–5 MHz US images of a small neurofibroma in the thigh with **d** fat-suppressed T2-weighted MR imaging correlation reveal a well-delineated oval mass (*arrows*) in continuity with the posterior femorocutaneous nerve (*arrowheads*). The tumor is characterized by concentric hypoechoic and hyperechoic layers (*1*, *2*, *3*) consistent with the sonographic target sign

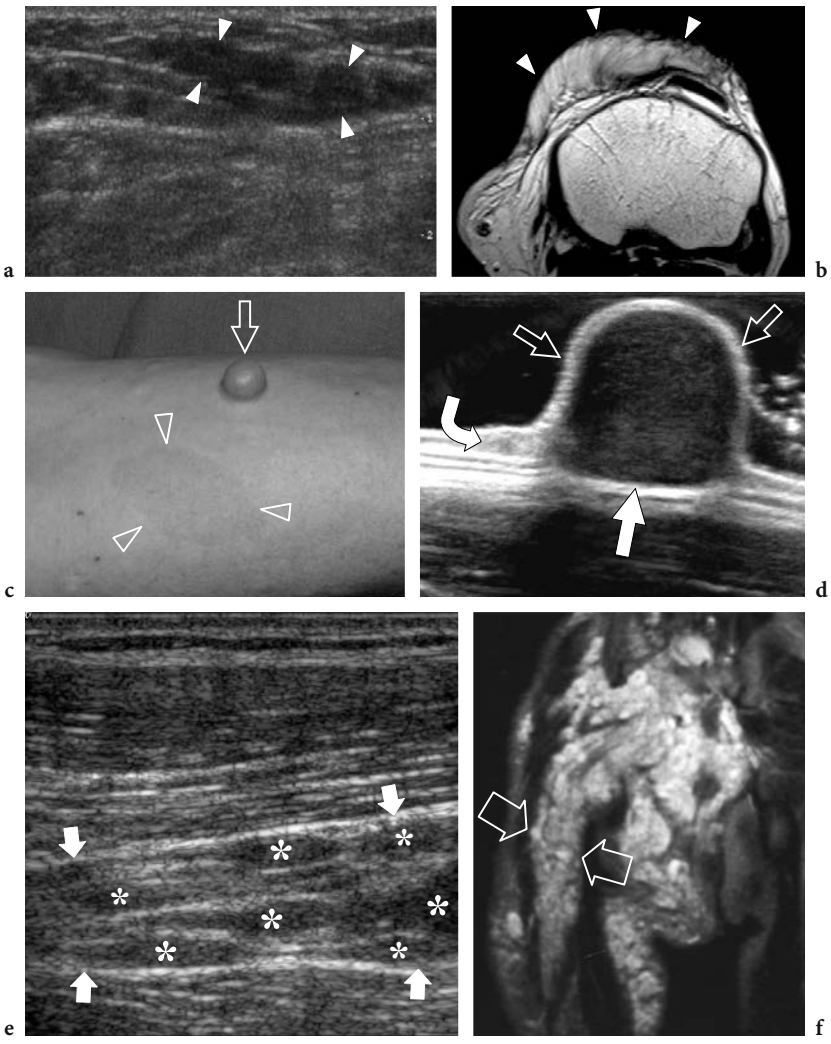

Fig. 4.22a–f. Neurofibroma: spectrum of US appearances. Three different cases. **a,b** Diffuse neurofibroma. **a** Transverse 12–5 MHz US and **b** T1-weighted MR images of the suprapatellar region in a 10-year-old child without neurofibromatosis show an ill-defined infiltrative mass (*arrowheads*) extending along the subcutaneous tissue of the anterior knee. **c,d** Sessile neurofibroma. **c** Photograph of the right forearm of a 43-year-old man with neurofibromatosis shows a sessile cutaneous neurofibroma (*arrow*) associated with café-au-lait spots (*arrowheads*). **d** The 17–5 MHz US image demonstrates the sessile neurofibroma as a superficial solid hypoechoic mass (*straight arrows*) arising from the dermis (*curved arrow*). **e–f** Plexiform neurofibromas. **e** Long-axis 12–5 MHz US image over the sciatic nerve in an 8-year-old child with intra- and extra-abdominal neurofibromatosis demonstrates multiple neurofibromas (*asterisks*) arising from individual fascicles of the sciatic nerve (*arrows*). **f** Coronal T2-weighted MR image of the pelvis and the proximal thigh shows innumerable neurofibromas along the course of a thickened and hyperintense sciatic nerve (*arrows*)

iner suspect that a nerve tumor is malignant are a sudden increase in size of a previously stable nodule and the presence of indistinct margins and adhesions of the mass with surrounding tissues. Especially in patients with type 1 neurofibromatosis, a rapidly enlarging nodule indicates the need for immediate biopsy.

Despite these differences, US cannot distinguish among schwannoma, neurofibroma, and malignant peripheral nerve sheath tumor (Lin and Martel 2001; Reynolds et al. 2004). US can contribute to the preoperative assessment of the extent of disease, by defining the relationship of the tumor to adjacent neurovascular structures and surrounding muscles and also by assisting surgical planning. After imaging assessment, fine needle aspiration biopsy of the mass can be confidently performed under US guidance. During biopsy, excruciating pain is frequently

triggered by the needle insertion. From the surgical point of view, schwannomas may be shelled out preserving nerve continuity and function (Murphey et al. 1999). In the postoperative setting, residual hypoechoic thickening of the nerve at the site of tumor resection is almost invariably seen with US: this should be regarded as a normal finding (Fig. 4.23). Recurrence is unusual. In contrast, surgical resection of neurofibromas requires sacrificing the parent nerve because the mass cannot be separated from the nerve fascicles, and subsequent nerve grafting is needed to preserve and restore function. Although surgical management may be acceptable in cutaneous neurofibromas, deep-seated lesions are usually managed conservatively to avoid functional deficit.

Type 1 neurofibromatosis (von Recklinghausen disease), a relatively common (1:2500–3000 births) inherited autosomal dominant disease related to an alteration of a gene on chromosome-17, presents with the typical clinical triad of cutaneous lesions (café-au-lait spots), skeletal deformities (scoliosis), and mental deficiency. Widespread involvement by neurofibromas of the localized, diffuse, and plexiform variety occurs with tumors arising from small dermal nerves and large deep-seated nerves. In neurofibromatosis, localized neurofibromas often involve the dermis and the subcutaneous tissue: when pedunculated, they are referred to as the "fibroma molluscum" (Fig. 4.22c,d) (Murphey et al. 1999). In plexiform (multinodular) neurofibromatosis – the pathognomonic form of the disease – innumerable neurofibromas are generated from the fascicles of a large nerve trunk, which is typically involved for a long segment together with its branches, leading to the so-called "bag-of-worms" appearance of the affected nerve at gross inspection and US imaging that results from the diffuse tortuous nerve thickening (Figs. 4.22e,f, 4.24) (Murphey et al. 1999). A disfiguring giant enlargement of the extremities may be associated, so-called elephantiasis neuromatosa (Murphey et al. 1999). Plexiform neurofibromas are indistinguishable from the more rare plexiform schwannomas which sporadically occur in children and young adults: the latter are not associated with type 1 neurofibromatosis and do not undergo malignant transformation (Fig. 4.25) (Ikushima et al. 1999; Katsumi et al. 2003).

4.1.8.2 Hemangioma and Non-Hodgkin Lymphoma

Nerve hemangiomas are extremely rare tumors arising from the endothelial lining of the endoneurium from which new vessels arise or infold within nerves from the perineural tissue. Most are recognized in children and young patients; there is no gender prevalence. The tumors tend to enlarge with age, or because of stimulating factors such as and trauma (Bilge et al. 1989). Nerve hemangiomas have a predilection for the median nerve; a persistent median artery has been advocated to explain this prevalence (Prosser and Burke 1987). Clinical findings include palpable nerve swelling at the distal forearm with or without symptoms of carpal tunnel syndrome. US reveals a markedly swollen median nerve containing large intraneural fluid-filled spaces separating the fascicles (Fig. 4.26). Typically, these anechoic spaces are oriented according to the long-axis of the nerve and compressible with the transducer. Color and power Doppler imaging show slow-flowing blood within them (Fig. 4.26c). Venous waveforms are pre-

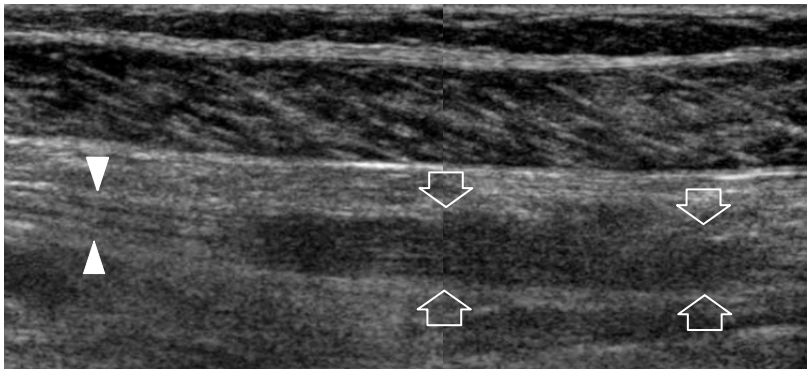

Fig. 4.23. Peripheral nerve sheath tumors: postsurgical findings. Long-axis 12–5MHz US image over the tibial nerve (*arrowheads*) at the mid-posterior leg in a 48-year-old woman who was previously operated on for schwannoma shows residual hypoechoic thickening (*arrows*) of the nerve at the site of tumor resection with loss of the fascicular echotexture. This finding was stable at 3 year follow-up. A split-screen image was used, with the two screens aligned for an extended field of view

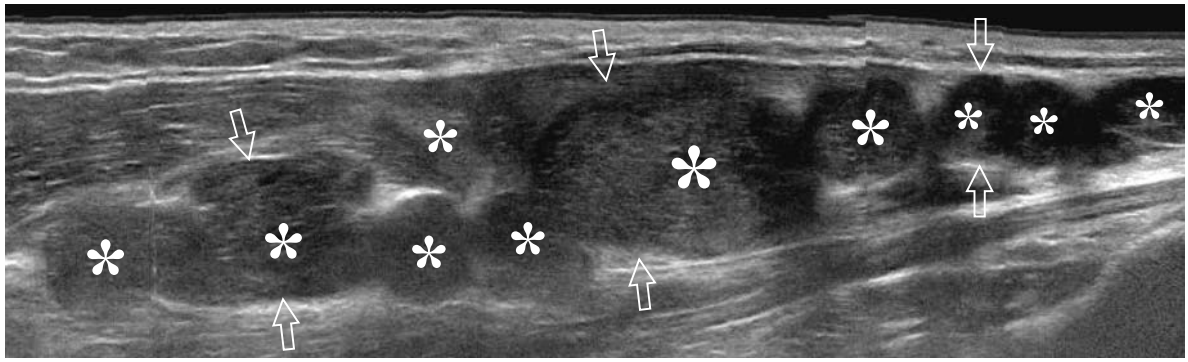

Fig. 4.24. Plexiform neurofibromatosis. Long-axis extended-field-of-view 17–5 MHz US image over the median nerve (*arrows*) at the forearm in a patient with neurofibromatosis shows multiple plexiform neurofibromas (*asterisks*), some of which have a central hyperechoic area representing the target sign. The median nerve is markedly enlarged and shows a convoluted multinodular appearance

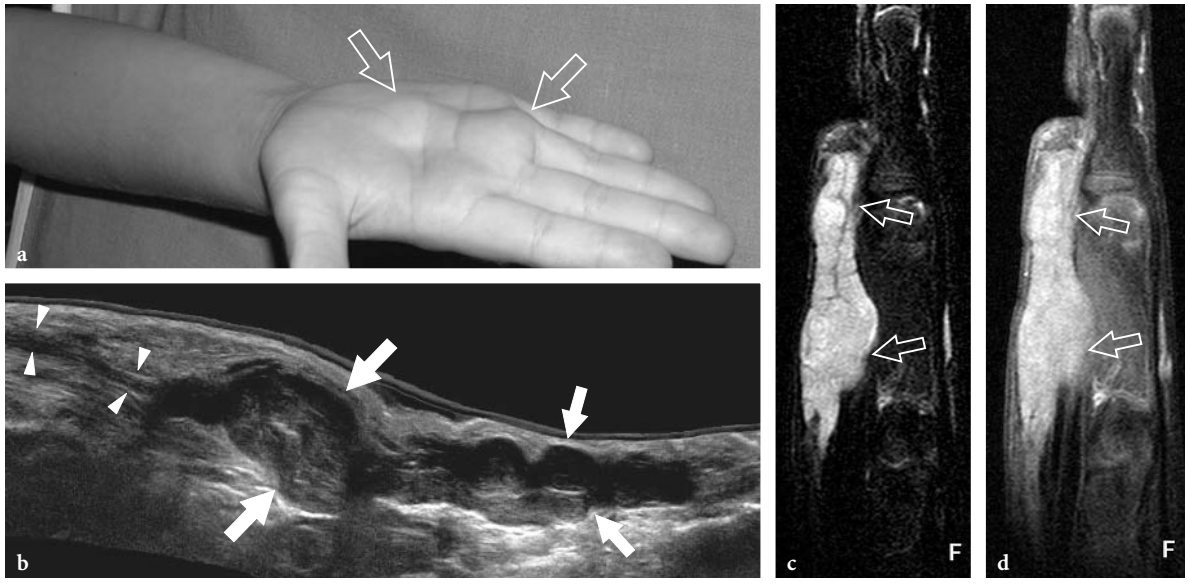

Fig. 4.25a–d. Plexiform schwannoma. **a** Photograph of the right hand of a 4-year-old child with an elongated palpable lump (*arrows*) on the palm, growing in between the third and fourth metacarpals. **b** Extended-field-of-view 17–5 MHz US image oriented along the long axis of the lump with fat-suppressed **c** T2-weighted and **d** postcontrast GRE T1-weighted MR imaging correlation demonstrates a multinodular hypoechoic mass (*arrows*) made up of swollen convoluted fascicles arising from the median nerve (*arrowheads*) and branching distally. The tumor appears hyperintense in T2 and after gadolinium administration

dominant at spectral Doppler analysis. Surgical neurolysis of nerve hemangiomas is not recommended because intraneural vessels are part of the "vasa nervorum" system and due to the intermingled distribution of vessels with fascicles. In symptomatic patients, carpal tunnel release may be performed to improve the clinical symptoms.

Primary non-Hodgkin lymphomas affecting peripheral nerves are very rare. Most involve the sciatic nerve and are the result of direct spread from adjacent tumors (Roncaroli et al. 1997). Peripheral neuropathy may also be appreciated in the absence of direct involvement of the nerve as a paraneoplastic manifestation of lymphoproliferative disorders. From the histopathologic point of view, the affected nerves show extensive neoplastic infiltration of the endoneurium and perineurium. The nerve fascicles are separated by diffuse infiltrates of neoplastic lymphoid cells contained within a thickened epineurium (Eusebi et al. 1990). US reveals a heterogeneous nerve mass with distortion and swelling of the individual fascicles (Fig. 4.27). The treatment usually consists of chemo- and radiotherapy (Pillay et al. 1988).

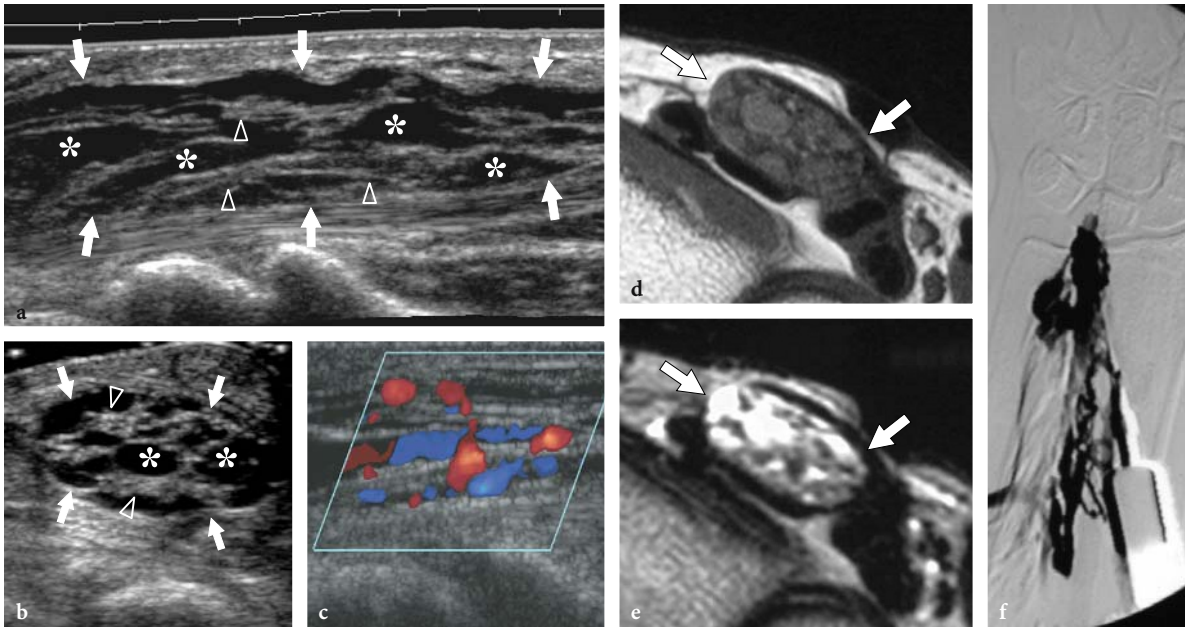

Fig. 4.26a–f. Hemangioma of the median nerve in a 40-year-old woman with carpal tunnel syndrome and a large intramuscular hemangioma extending through the flexor muscles of the forearm down to the carpal tunnel. The patient underwent release of the retinaculum and partial resection of the mass with removal of the flexor digitorum superficialis muscle. **a** Long-axis and **b** short-axis 17–5 MHz US images obtained at the distal radius show an enlarged median nerve (*arrows*) with intranervous abnormal fluid-filled spaces (*asterisks*) running alongside the fascicles (*arrowheads*). **c** Longitudinal color Doppler 12–5 MHz US image reveals slow-flowing blood within the intraneural spaces indicating a hemangioma. Vessels are compressible and exhibits venous waveforms. **d,e** Correlative transverse **d** T1-weighted and **e** T2-weighted MR images show increased T2 signal intensity in the epineurium surrounding the fascicles of the median nerve (*arrows*), due to the presence of abnormal vessels within the nerve substance. **f** Digital subtraction angiography confirms the presence of a venous network in the median nerve

4.1.8.3 Intraneural Ganglia

The incidence of intraneural ganglia is relatively low, affecting most frequently the common peroneal nerve (Yamazaki et al. 1999). This nerve originates at the apex of the popliteal fossa from the sciatic nerve and moves downward to the fibular head, where it divides into its two terminal branches: the deep and the superficial peroneal nerve. Around the fibular neck, the deep peroneal nerve gives off a small recurrent articular branch to supply the capsule of the superior tibiofibular joint. The capsular ending of this small branch may lead to the development of intraneural ganglia (Spinner et al. 2003, 2005). In fact, this branch serves as a conduit for cyst fluid to pass from the joint space into the nerve (Spinner et al. 2003). The joint fluid dissects the epineurium among the fascicles and moves toward the deep peroneal nerve, the common peroneal nerve and even the sciatic nerve, forming an elongated intraneural cyst. As described in Chapter 14, intraneural ganglia do not have a fibrous capsule or a synovial lining and must be differentiated from the more common extraneural ganglia. As an extension of the superior tibiofibular joint, they appear as spindle-shaped cystic masses contained within the nerve sheath that grow in the space between the epineurium and the nerve fascicles (Martinoli et al. 2000b).

4.1.8.4 Nerve Encasement by Extrinsic Neoplasms

Extrinsic soft-tissue tumors may involve normal nerves by contiguity. They may either displace and compress the nerve at the periphery of the mass without infiltrative signs or can incorporate the nerve. In the first instance, the integrity of the nerve can be preserved at surgery after removal or debulking of the mass. In the latter, the surgical procedure is obliged to sacrifice the encased nerve together with the tumor (Fig. 4.28). US may aid in assessing the extent of tumor preoperatively, and in defining the exact relationship of the mass with the nerve and its divisional branches (Fig. 4.29).

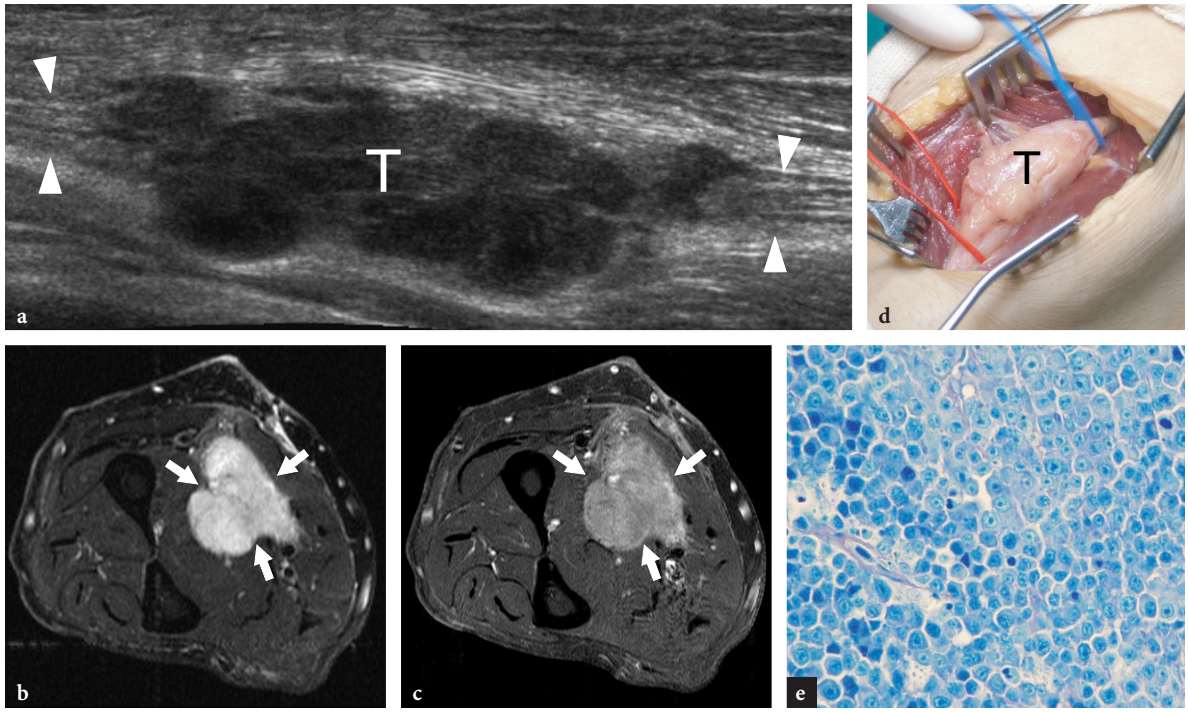

Fig. 4.27a–e. Primary non-Hodgkin lymphoma of the median nerve in a 62-year-old man with a slowly growing painless soft-tissue mass at the mid-forearm. **a** Extended-field-of-view 17–5 MHz US image with transverse fat-suppressed **b** T2-weighted and **c** gadolinium-enhanced T1-weighted MR imaging correlation demonstrates a lobulated multinodular hypoechoic mass (*T*) in continuity with the fascicles of the median nerve (*arrowheads*), an appearance quite different from that of peripheral nerve sheath tumors. The tumor (*arrows*) appears diffusely hyperintense in T2 and after gadolinium administration. **d** Gross surgical view confirms the neurogenic nature of the mass (*T*). **e** Histologic specimen shows diffuse involvement of the nerve tissue by lymphoid elements. Original magnification ×800

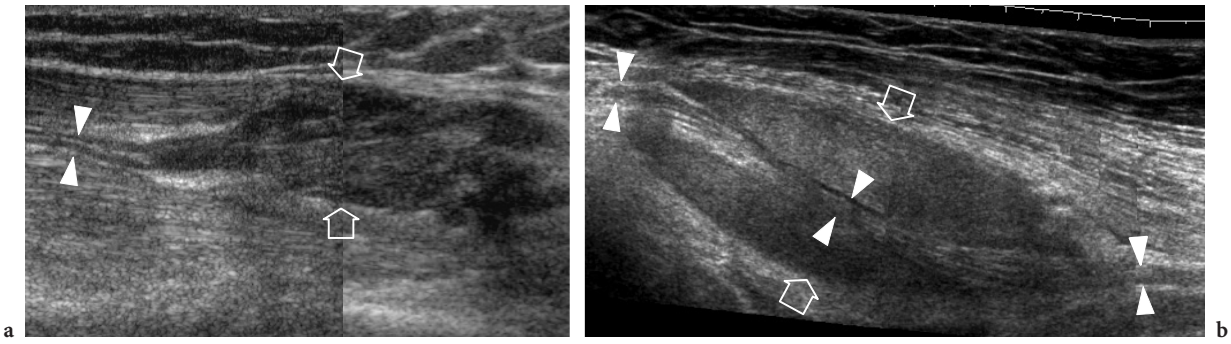

Fig. 4.28a,b. Nerve involvement by extrinsic tumors. Two different cases. **a** Longitudinal 12–5 MHz US image over the lateral knee in a 25-year-old patient with relapsed desmoid tumor after surgery demonstrates the peroneal nerve (*arrowheads*) incorporated by the mass (*arrows*). **b** Oblique longitudinal 12-5 MHz US image over the mid-distal third of the arm in a 67-year-old woman with liposarcoma shows a long segment of the radial nerve (*arrowheads*) encased by the neoplasm (*arrows*). In both cases, surgery was obliged to sacrifice the involved nerve

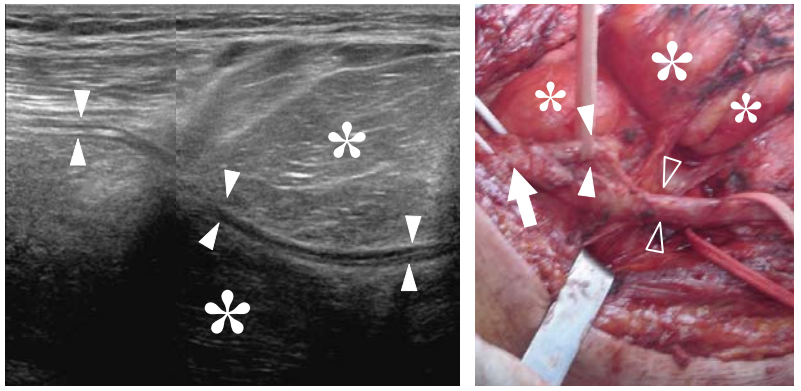

Fig. 4.29a,b. Nerve involvement by extrinsic tumors. **a** Oblique longitudinal 12-5 MHz US image over the popliteal fossa demonstrates a large lipomatous mass (*asterisks*) encasing the peroneal nerve (*arrowheads*). A split-screen image was used, with the two screens aligned for an extended field of view. **b** Gross surgical view shows the bifurcation of the sciatic nerve (*arrow*) into the tibial (*open arrowheads*) and the peroneal (*white arrowheads*) nerves. This latter nerve can be seen infolding within the mass (*asterisks*). Pathologic examination revealed a liposarcoma

4.2 Blood Vessels

An in-depth complete treatise on the arteries and veins running in the limbs and extremities and related-pathology is beyond the scope of a book on the musculoskeletal system. Here, we will focus on general aspects of vascular pathology related to musculoskeletal diseases. Some concepts are specifically addressed in other chapters of the book. The analysis of the proper vascular pathology of limb arteries and veins, such as atherosclerotic disease and venous insufficiency, is more appropriately dealt with in other textbooks and specific literature (Polak et al. 1989; Edwards and Zierler 1992; Foley et al. 1989; Fraser and Anderson 2004).

4.2.1 Histologic Considerations

Based on their histologic architecture, the arteries can be divided into four different groups: elastic arteries, medium-sized muscular arteries, small arteries, and arterioles (i.e. the radial and ulnar arteries belong to the medium-sized muscular group). Elastic arteries are the largest in the body; they expand when the heart contracts and return to a normal caliber in diastole. Muscular arteries are small and middle-sized vessels with a relatively narrow lumen and thick walls consisting of circumferentially arranged smooth muscle fibers which restrict the lumen when they contract. The tonus of the smooth muscle component depends on the autonomic nervous system and is responsible for the round cross-sectional shape of the arteries, for blood pressure levels, and for regulatory functions of blood flow (i.e. increased flow volume in the skeletal muscles during exercise). The arterial wall is composed of three concentric layers: the intima (inner tunica) containing the endothelial lining; the media (intermediate tunica) housing smooth muscle tissue; and the adventitia (outer tunica) characterized by fibrous tissue merging with the loose connective space around the vessel (Fig. 4.30a). In a muscular artery, the lamina elastica interna lies between the intima and the media, whereas the lamina elastica externa separates the media from the adventitia.

Compared with the arteries, veins have thinner walls and larger lumens. One of their main function is to store blood, and they need muscle to push the blood back to the heart. Because the venous walls may collapse, the vessel shape varies depending on the surrounding tissue conditions, including the subject's positioning and gravity. In contrast to the arteries, the layering of the venous wall is not so distinct: the intima is very thin (only the largest veins contain discrete amount of subendothelial connective tissue); the media is thinner than the adventitia, and the two layers blend into each other. Peripheral veins may be double or multiple when accompany a medium-sized artery and are, in general, more variable than the arteries themselves, with anastomoses very often occurring between them. Many small to medium-sized veins contain valves (Fig. 4.31a).

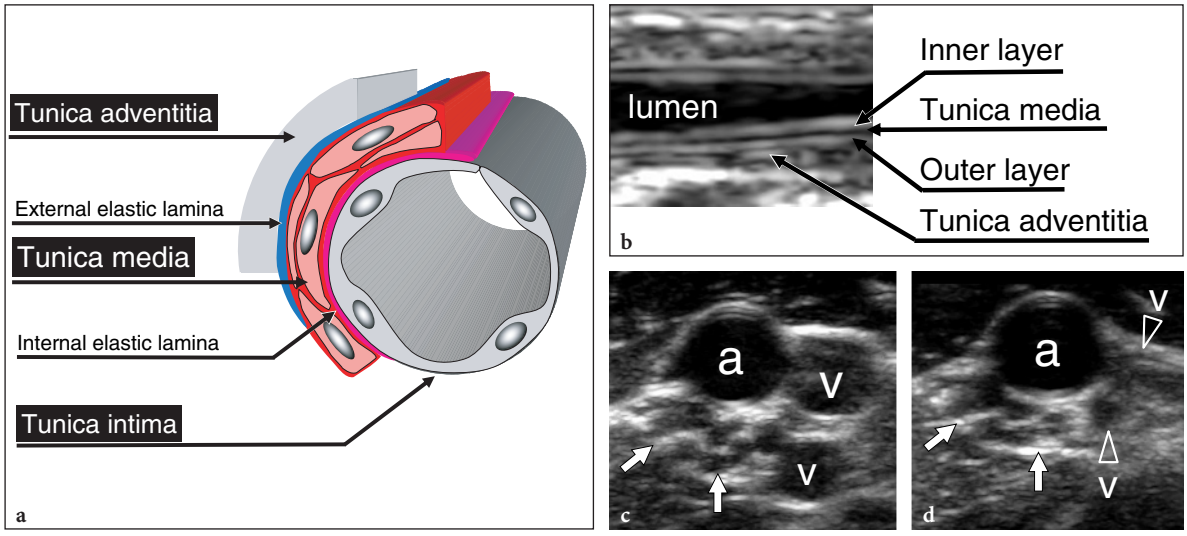

Fig. 4.30a–d. Anatomy of muscular arteries. **a** Schematic drawing of a cross-sectional view through a small- to medium-sized muscular artery illustrates the histologic organization of the vessel wall consisting of three concentric layers. From internal to external, they are: the tunica intima, composed of endothelium; the tunica media, characterized by smooth muscle cells; and the tunica adventitia, composed of loose connective tissue in continuity with the perivascular spaces. The intima is separated from the media by the lamina elastica interna; and the media from the adventitia by the lamina elastica externa. **b** Long-axis 17–5 MHz US image of a small artery shows the ordered structure of the arterial wall made up of a combination of hyper- and hypoechoic layers. They are: an inner echogenic layer due to the interface of blood with the intima and the lamina elastica interna; an intermediate hypoechoic layer due to the tunica media; an outer echogenic layer given by the acoustic interface between the lamina elastica externa and the adventitia. **c,d** Short-axis 17–5 MHz US images over the major neurovascular bundle of the arm obtained **c** without and **d** with probe compression. A common hyperechoic connective sheath invests one artery (*a*), two satellite veins (*v*), and a nerve (*arrows*). The artery can be distinguished from the adjacent veins on the basis of its more rounded cross-sectional profile, multilayered wall, pulsatility (not shown), and because it does not collapse while applying transducer pressure over it

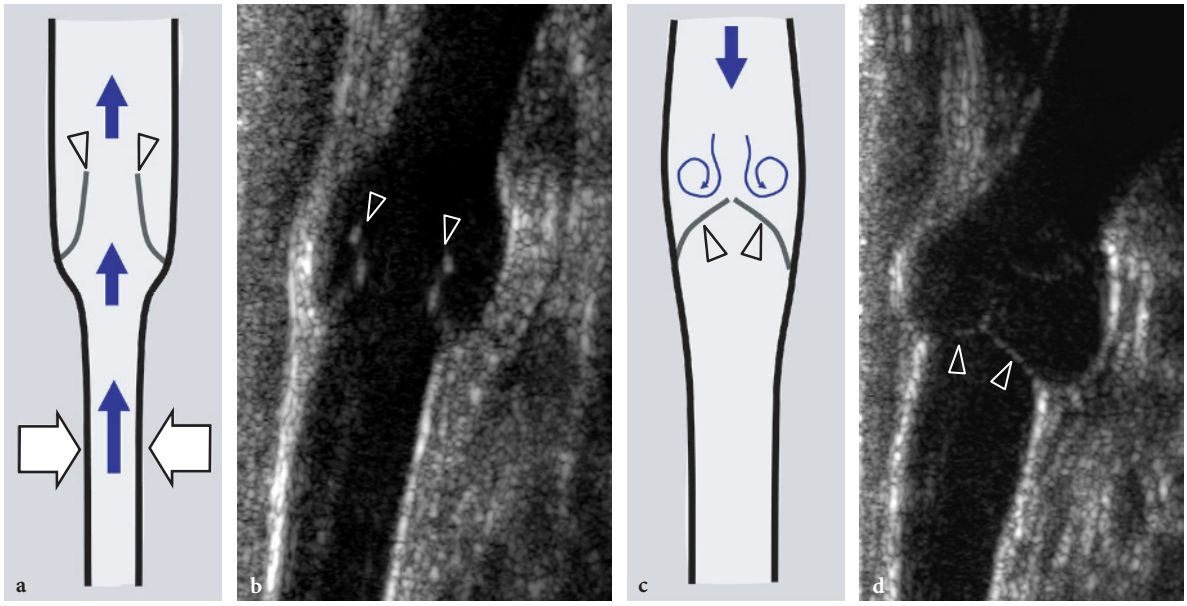

Fig. 4.31a–d. Venous valves. **a,c** Schematic drawings and correlative **b,d** long-axis 12–5 MHz US images over a peripheral vein illustrate the hemodynamic effects of a valve on venous blood flow. **a,b** During contraction of calf muscles (*white arrows*), the cusps (*arrowheads*) of the valve open, allowing blood (*blue arrows*) to flow toward the heart. **c,d** Once the muscle action has ceased, flow tends to reverse, closing the cusps of the valve. Closure of the valve impedes blood to direct it backward

These are loose, pocket-shaped folds of the intima, which extend into the lumen of the vein. The opening of the cusps prevents backflow of blood and encourages flow toward the heart. Blood flowing toward heart passes the pockets (Fig. 4.31a,b); if the flow reverses, blood fills the pockets thus occluding the lumen of the vein and preventing the pooling of blood (Fig. 4.31c,d). When a subject is standing, the venous return from the legs depends mainly on the activity of calf muscles, the so-called calf pump.

4.2.2 Normal US Anatomy and Scanning Technique

Because the limb arteries are relatively superficial, very good quality US images are usually obtained with the transducers used for musculoskeletal applications. Similar to other applications, selection of the appropriate transducer frequency depends on the patient's build and the depth of the vessel to be examined. Changing the machine settings from a musculoskeletal application to a vascular-specific setting and lowering the gain may help to reduce artifactual speckles within the vessel lumen that may generate confusion with thrombus. In normal states, limb arteries appear as pulsatile structures: pulsatility is better appreciated on short-axis planes during prolonged observation. This sign is usually sufficient to assess limb arteries during a conventional study of the musculoskeletal system for unrelated purposes.

Based on correlative microdissection studies and the use of high-resolution intravascular probes, US demonstrates the normal wall of a small to medium-sized muscular artery as a three-layered structure. An inner bright acoustic linear echo derives from the interface of blood with the intima and the lamina elastica interna, and an outer echogenic layer is produced by reflection at the interface between the lamina elastica externa and the adventitia (Fig. 4.30b) (Chong et al. 1993; Siegel et al. 1993). Being primarily composed of smooth muscle, the tunica media appears as a mid-hypoechoic band intervening between the two echogenic layers (Chong et al. 1993; Siegel et al. 1993). In contrast, the wall of elastic arteries, whose media have a high elastin content, appears uniformly echogenic (Chong et al. 1993; Siegel et al. 1993; Martin et al. 1997).

When vascular disease is suspected, color Doppler imaging and spectral Doppler analysis can complement gray-scale findings to determine patency and vessel narrowing. As a rule, Doppler examination should be performed along the longitudinal axis of the vessels with a Doppler angle of 60° or less (Fig. 4.32a). Because most vessels of the extremities course parallel to the skin, beam steering should be used as a default setting to obtain adequate Doppler angles. At rest, spectral Doppler analysis of flow waveforms and color Doppler imaging of the upper and lower limb arteries demonstrate a characteristic pattern of high distal resistance (Fig. 4.32b). In response to exercise and muscle activation, vasodilation usually produces a higher forward flow

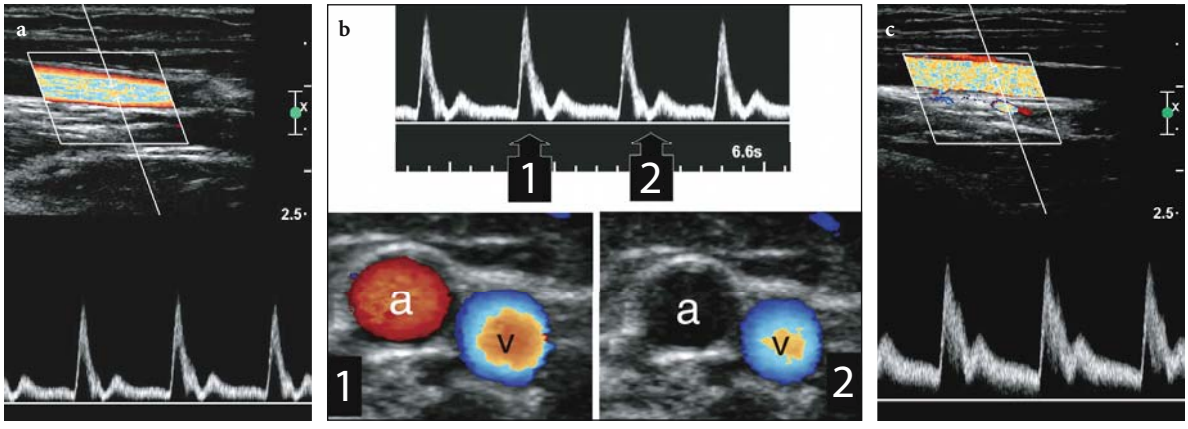

Fig. 4.32a–c. Normal Doppler imaging findings in the brachial artery. **a** Pulsed Doppler analysis shows normal high-resistance pulsatile flow with oscillations in diastole. A steered color box is used to obtain an adequate Doppler angle and clear-cut Doppler tracings. **b** Color Doppler imaging appearance of flow in the high-resistance brachial artery (*a*). There is evidence of color flow signal in systole (*1*) but not in the early diastolic phase (*2*). Continuous blood flow is detected in the adjacent brachial vein (*v*) with complete filling of the vessel lumen, indicative of patency. **c** Following repeated fist clenching, the resulting vasodilation produces a higher forward flow throughout the cardiac cycle, particularly in diastole

throughout the cardiac cycle, particularly in diastole, reflecting decreased resistances (Fig. 4.32c).

Unlike the arteries, limb veins have very thin echogenic walls that are often indistinguishable from the surrounding echogenic spaces, particularly when the vessel is collapsed (Fig. 4.30c,d). The venous system is examined by placing the probe perpendicular to the direction of vascular flow using the so-called compression technique (compression sonography), because noncompressibility is the most sensitive and specific sign of venous thrombosis (Cronan et al. 1987; Fraser and Anderson 2004). The reason why compression is applied in the transverse plane is related to the fact that the probe may slide off the vessel in the longitudinal axis, potentially resulting in a false-negative finding (Chin et al. 2005).

Initially, light pressure is used so as not to collapse the vein (Fig. 4.33a). With the probe straddling both artery and vein, further pressure is subsequently applied. If the vein is patent, the walls collapse and appose each other completely (Fig. 4.33b). When the pressure is released, the lumen of the vein returns to normal. If the vein contains clots, it will not collapse but remains distended when applying probe pressure (Fig. 4.33a,b). In lower limb veins, Doppler imaging and spectral analysis reveal monophasic venous flow rather than triphasic waveforms. In contrast, upper limb veins demonstrate more pulsatile flow because of their closer proximity to the heart (Chin et al. 2005). The use of low velocity (3–6 cm/s) and low filter settings is mandatory to avoid artifactual venous occlusion. In normal conditions, venous flow should be increased on inspiration and reduced in expiration. Absence of variation may indicate a more proximal obstructive or compressive lesion, and further assessment in required. The Valsalva maneuver can also be used as a means to evaluate the more proximal venous system. The application of distal augmentation (e.g., squeezing the calf to evaluate the popliteal vein, squeezing the foot to evaluate the tibial veins) leads to an increase in the color and spectral Doppler signal (Fig. 4.33c,d). This phenomenon indicates that the venous segments between the compression point and the position of the probe are patent. Venous dilatation may occur in the presence of acute venous thrombosis.

Among anatomic variants, duplication of veins, especially at the femoral (20%) and popliteal (35%) level, is common. In this instance, veins are generally smaller than in a single system and may be potential source of error at continuous-wave Doppler analysis.

4.2.3 Musculoskeletal-Related Vascular Disorders

As already stated, we will focus here on a brief description of the vascular pathology related to traumatic injuries or specific musculoskeletal diseases

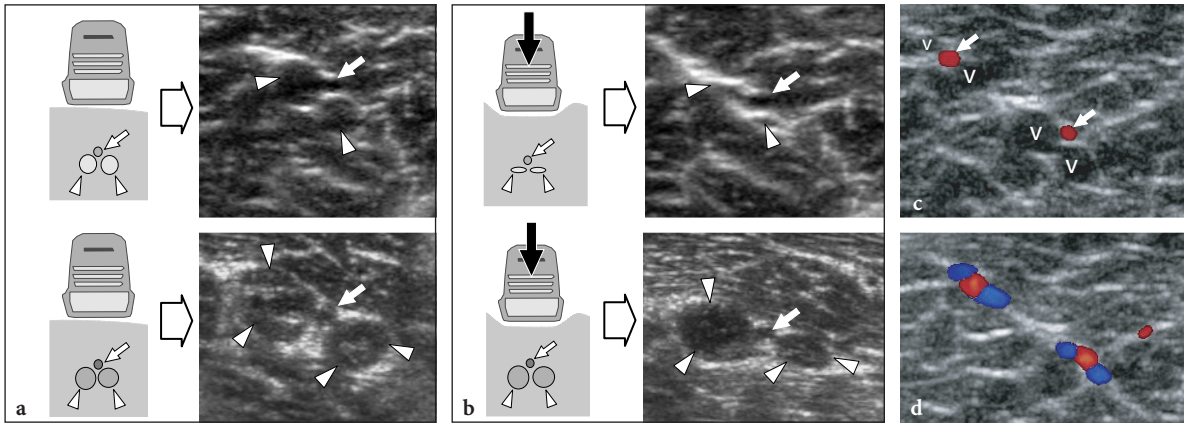

Fig. 4.33a-d. Dynamic compression technique to assess vein patency. **a,b** Schematic drawings and corresponding short-axis 17–5 MHz US images obtained in two different patients over patent (*upper images*) and thrombosed (*lower images*) gemellary veins (*arrowheads*). *Arrow* indicates the gemellary artery. **a** The probe is first held transverse to the vessels without applying pressure over them. Both patent and thrombosed veins show a rounded profile. Some internal echoes reflecting blood clots are observed in the lower image. **b** Applying pressure with the probe over the veins causes collapse of the anterior and posterior walls when they are patent (*upper image*). On the contrary, the veins filled with thrombus remain distended. **c,d** Distal augmentation maneuver. **c** Color Doppler US image obtained at rest over normal gemellary veins does not reveal spontaneous blood flow in these veins (*v*). Observe the spontaneous color flow in the gemellary arteries (*arrows*). **d** Following distal manual squeezing of the calf, blood flow becomes apparent in the gemellary veins. This augmentation maneuver suggests patency of the calf veins

which must be known by the sonologist when performing a US study of the musculoskeletal system. Other vascular pathology, even if relevant, has been omitted as outside the aims of this book.

4.2.3.1 Arterial Disorders

Because of their superficial location and close apposition to the bones, the arteries of the limbs and extremities are particularly vulnerable to traumatic injuries. Based on its pathomechanism, arterial trauma can be arbitrarily subdivided into three main types: acute direct injuries following a penetrating wound by a sharp object or blunt arterial lacerations related to major stretching or contusion trauma (including high-grade sprains, bruising, dislocated joints and fracture-dislocations near arteries – such as supracondylar humeral fractures for the brachial artery, glenohumeral dislocations for the axillary artery, supracondylar femoral fractures for the popliteal artery, and knee dislocation for the posterior tibial artery); chronic repeated microtrauma causing progressive damage to the vessel wall that may lead to pseudoaneurysms, aneurysms, and vessel occlusion; and iatrogenic injuries resulting in either thrombosis or local hemorrhage. When major arterial trunks of the limbs are involved, direct traumatic injuries are clinical emergencies and, in most cases, require immediate surgical repair to avoid acute limb ischemia, hypotensive shock, and death related to blood loss (Davison and Polak 2004). Doppler US has been advocated for the diagnosis of acute arterial trauma to the extremities in an emergency setting, but its sensitivity is lower than that of CT angiography (Fry et al. 1993; Knudson et al. 1993; Miller-Thomas et al. 2005; Rieger et al. 2006). Similar to MR imaging, color Doppler US has substantial limitations in this field, related to the considerable amount of time needed to make the diagnosis. In addition, color Doppler imaging is operator-dependent, may be inadequate in the evaluation of arterial flow distal to an arterial injury, is susceptible to confusion created by collateral vessels, and may be unsuitable in patients with open wounds (Rieger et al. 2006).

Color Doppler imaging seems more useful for identifying and monitoring minor arterial injuries occurring during trauma that do not require specific immediate operative management – such as intimal lesions, pseudoaneurysms, and minor vessel occlusions – in order to assess whether they resolve or progress (Schwartz et al. 1993). Similarly, gray-scale US and Doppler imaging techniques seem more relevant for identifying incidental arterial damage secondary to chronic microtrauma and overuse syndromes. These lesions typically occur in the hand, where the branches of the ulnar artery can be pinched between the skin and the underlying hamate as the result of repeated external trauma against the palm (Fig. 4.34). This condition, which is commonly referred to as "hypothenar hammer syndrome," results in intimal injury, thrombosis or aneurysm with subsequent digital ischemia, pain or a palpable mass in the hand (see also Chapter 10) (Okereke et al. 1999; Liskutin et al. 2000; Velling et al. 2001). Similar vascular abnormalities may occur at the level of the dorsalis pedis artery following repeated blunt trauma over the dorsum of the ankle and midfoot (Yamaguchi et al. 2002; Ozdemir et al. 2003). In these cases, US and Doppler techniques should be the first-line imaging modality. Digital subtraction angiography or contrast-enhanced MR-angiography may still be required by the vascular surgeon for precise preoperative planning. Other uncommon causes of closed arterial damage associated with abnormalities of the musculoskeletal system are related to anatomic variants, such as: injury to the popliteal artery due to osseous abnormalities in patients with hereditary multiple exostoses (see Chapter 14) (Chamlou et al. 2002); popliteal artery entrapment syndrome, produced by anomalous proximal insertion of the medial head of the gastrocnemius (Fig. 4.35) (see Chapter 14) (Wright et al. 2004); and brachial artery entrapment in the arm secondary to the presence of a supracondylar process and the Struthers ligament, so-called supracondylar process syndrome (see Chapter 7) (Talha et al. 1987).

As regards iatrogenic injuries, procedures of arterial catheterization may be responsible for vascular dissections, soft-tissue hematomas, pseudoaneurysms, and arteriovenous fistula formation (Clevert et al. 2005; Schwartz et al. 1991). These lesions are typically located at the puncture site, including the groin for the femoral artery and its divisional branches (see Chapter 12) (Roubidoux et al. 1990; Helvie et al. 1988) and the medial arm for the brachial artery (see Chapter 7) (Chuang et al. 2002). Compression-based femoral and median neuropathy is a well-established complication of hematomas and pseudoaneurysms following arterial catheterization (see Chapter 7) (Jacobs et al. 1992; Chuang et al. 2002). Color Doppler imaging is useful in differentiating complications of femoral

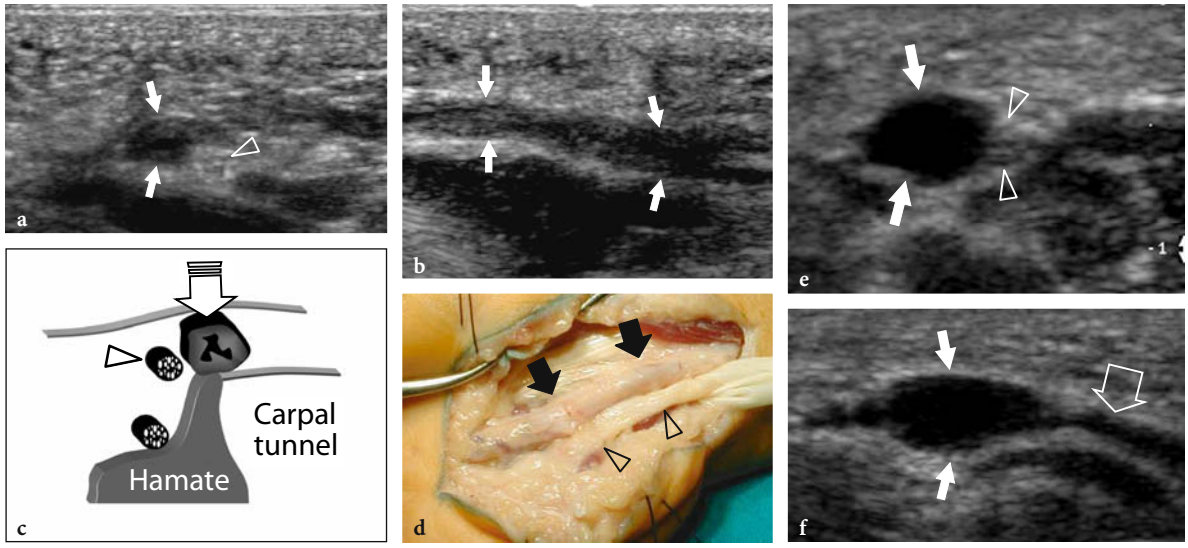

Fig. 4.34a–f. Hypothenar hammer syndrome. Two different cases of manual workers – one a car mechanic, the other a weightlifter – who had occupational hammering in their right hands. **a–d** Occlusion of the ulnar artery. **a** Transverse and **b** longitudinal 15–7 MHz US images over the hypothenar eminence with **c** schematic drawing and **d** gross surgical view correlation show complete occlusion of the ulnar artery (*arrows*) at the point where it courses adjacent to the hamate hook. Note the adjacent uninjured sensory branch of the ulnar nerve (*arrowhead*). Operative view demonstrates a thickened pale artery coursing adjacent to the ulnar nerve. The patient had ischemic symptoms in the fourth and fifth fingers. **e,f** Aneurysm of the ulnar artery. **e** Transverse and **f** longitudinal 12–5 MHz US images over the hypothenar eminence demonstrate an aneurysm (*white arrows*) of the ulnar artery (*large open arrow*). There are no echoes evident in the lumen, indicating absence of thrombus. The patient complained of only mild pain over the aneurysm. *Arrowheads*, sensory branch of the ulnar nerve

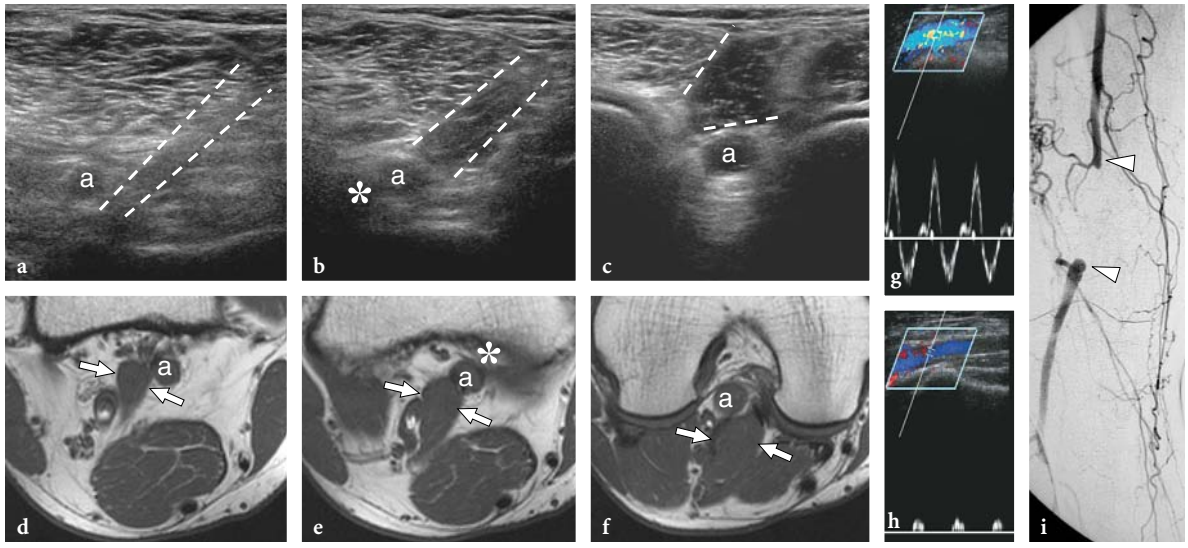

Fig. 4.35a–i. Popliteal artery entrapment syndrome. **a–c** Series of transverse 17–5 MHz US images of the popliteal fossa with **d–f** T1-weighted MR imaging correlation in a 45-year-old man with exercise-induced claudication of his right lower extremity demonstrate an anomalous medial course of the popliteal artery (*a*), which passes from medial to lateral across an abnormal muscle band (*dashed line* in **a-c**, *arrows* in **d-f**) lying in the popliteal fossa. At color Doppler imaging (not shown), the vessel occlusion initiated at the point where the artery is closely apposed to the posteromedial corner of the medial femoral condyle (*asterisk*) and is, therefore, vulnerable to compression by the anomalous muscle. MR imaging allowed this muscle abnormality to be classified as type 2. **g,h** Spectral Doppler analysis performed **g** at the upper-popliteal artery level and **h** downstream in the tibial artery at the proximal leg reveals **g** normal pulsatile flow cranial to the occlusion and **h** dampening of the distal flow waveforms. **i** Anteroposterior digital subtraction angiography shows segmental occlusion (*arrowheads*) of the popliteal artery with collateral filling through the geniculate arteries

artery catheterization, such as hematoma, pseudoaneurysm, and arteriovenous fistula. It demonstrates arterial pseudoaneurysm as a perivascular sac with thickened echogenic walls (mural thrombus) containing swirling flow with alternating red and blue colors (Fig. 4.36a–c). In general, the neck connecting the artery with the pseudoaneurysm is better recognized on color Doppler imaging than on gray-scale US (Schwartz et al. 1991). At Doppler spectral analysis, blood flow in the neck exhibits bidirectional high velocities as blood enters the cavity from the damaged artery in systole (flow displayed above the baseline) and exits in diastole (flow displayed below the baseline), the so-called "to-and-fro" signal (Fig. 4.36d) (Sacks et al. 1989). On the other hand, characteristic findings of arteriovenous fistulas include: visible connection between artery and vein, multicolored (mosaic pattern) speckled mass at the fistula site, spreading of color pixels into the perivascular soft tissues, high diastolic flow in the arterial waveform proximal to the fistula site, decreased flow in the artery caudal to the fistula, and high-velocity turbulent flow, sometimes with a pulsatile component, in the efferent vein (Helvie and Rubin 1989; Roubidoux et al. 1990). US-guided procedures to treat pseudoaneurysms with direct probe compression and thrombin injection are described elsewhere (see Chapter 12). In the postoperative setting, US and Doppler techniques have proved valuable in evaluating by pass grafts to detect the onset of early failure, including stenoses, thrombosis, and infectious collections (Fig. 4.37).

4.2.3.2 Venous Disorders

Direct trauma to the deep and superficial venous system only occasionally produces a vascular lesion, such as an aneurysm or a vein occlusion. Although rare, the possibility of a venous aneurysm should, however, be taken into account so as not to confuse an aneurysm with either a ganglion cyst (when patent) or a solid soft-tissue mass (when thrombosed). Demonstration of the continuity of the dilated venous segment with a superficial, even small, vein and blood flow detected within the mass may help the diagnosis (Fig. 4.38a–d). When thrombosed, venous aneurysms may be a diagnostic challenge because they appear as nonspecific solid avascular masses (Fig. 4.38e). Post-traumatic vein thrombosis may occasionally be encountered following muscle strains as a result of stretching of the vessel walls. This kind of trauma typically occurs in the infrapopliteal veins (the gemellary veins are the most commonly involved) of patients with tennis leg lesion (see Chapter 15) (Delgado et al. 2002). Post-traumatic muscle edema and hematoma may also produce compression and then occlusion of low-pressure intramuscular veins. Similarly, pro-

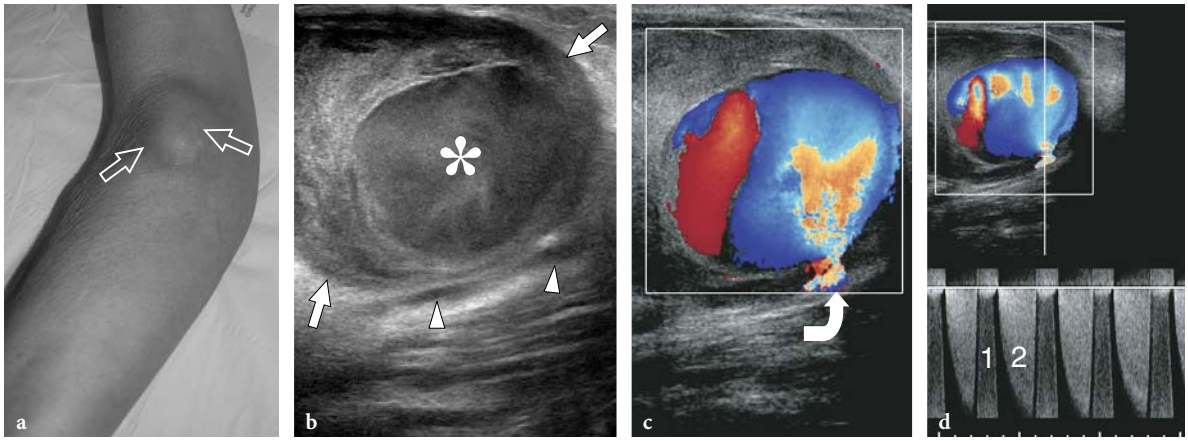

Fig. 4.36a–d. Iatrogenic pseudoaneurysm of the brachial artery. **a** Photograph of the anterior right elbow of a 72-year-old woman presenting with an enlarging pulsatile soft-tissue lump (*arrows*) that developed after a vein cannulation procedure. Transverse **b** gray-scale and **c** color Doppler 17–5 MHz US images over the lump reveal a large complex mass (*straight arrows*) with thickened walls and a central cavity filled with whirling flow (*asterisk*) consistent with a pseudoaneurysm of the brachial artery (*arrowheads*). The slow flow in the pseudoaneurysm makes blood echogenic at gray-scale imaging. Color Doppler imaging demonstrates continuity of the pseudoaneurysm cavity with a displaced brachial artery by means of a thin neck (*curved arrow*). **d** Spectral Doppler analysis obtained in the communicating tract displays bidirectional velocities as the forward flow (*1*) in systole is ejected (*2*) in diastole

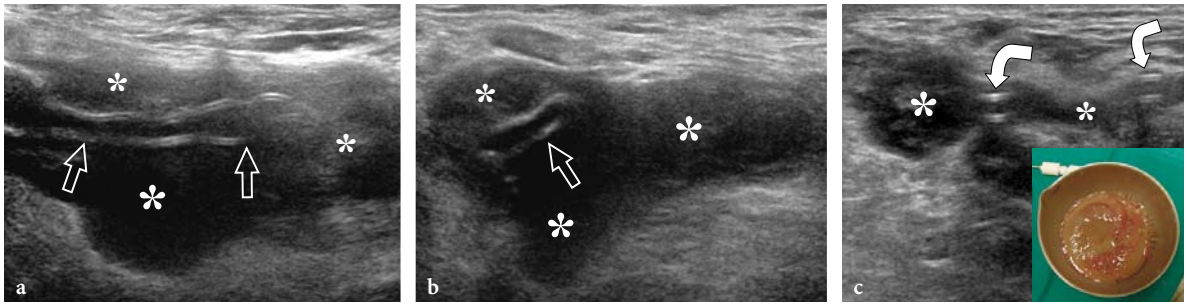

Fig. 4.37a–c. Abscess around a bypass graft. **a** Long-axis and **b** short-axis 17–5 MHz US images over an occluded aorto-femoral bypass graft (*arrows*) in a 70-year-old diabetic patient with amputated lower leg and clinical signs of sepsis. Note the shrunken appearance of the graft surrounded by a fluid collection (*asterisks*). **c** Preoperative percutaneous drainage of the collection. The catheter (*curved arrows*) is seen inside the almost empty abscess (*asterisks*). As shown in the *insert*, aspiration resulted in purulent material

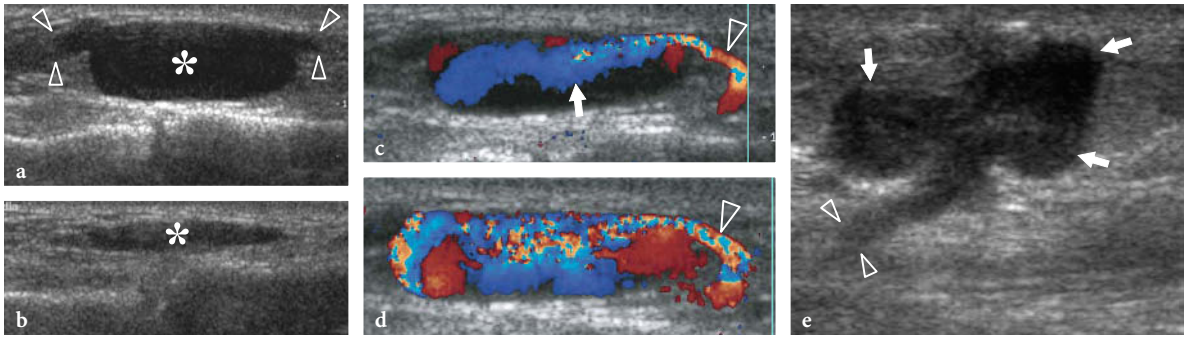

Fig. 4.38a–e. Venous aneurysms. Two different cases. Long-axis **a,b** gray-scale and **c,d** color Doppler 12–5 MHz US images obtained **a,c,d** without and **b** with probe compression over a compressible soft-tissue mass of the dorsum of the mid-foot in a patient with healed mid-tarsal fractures reveal a fluid-filled oval lesion (*asterisks*) connected at its opposite ends to a small superficial vein (*arrowheads*). As shown in **b**, the mass is fully compressible without internal thrombus. This sign, together with demonstration of the venous ends and of internal blood flow at color Doppler imaging, may avoid confusion with ganglion cysts. While releasing probe compression, blood flow (*arrow*) can be seen entering the aneurysm from the parent vein (*arrowhead*) to completely fill its cavity. **e** Thrombosed superficial varicose vein. Sagittal 12–5 MHz US image over the posteromedial aspect of the leg shows a polycyclic hypoechoic mass (*arrows*) in continuity with a thin pedicle (*arrowheads*) directed toward depth, an appearance nonspecific at US examination. After surgical resection, this mass proved to be a thrombosed varix

longed absence of contracture of the calf muscles as a result of local pain and post-traumatic immobilization may be implicated as a possible cause of venous thrombosis.

In the lower limb, compression US and color Doppler imaging can easily diagnose deep venous thrombosis and distinguish a vascular problem from other musculoskeletal conditions that may mimic it, including a ruptured Baker cyst (see Chapter 14) or a post-traumatic hematoma (see Chapter 15). The classic description of venous thrombosis is that of an enlarged vein with thickened walls containing echogenic material with multiple surrounding collateral vessels (Murphy and Cronan 1990). Based on the imaging findings, US can distinguish complete occlusive (Fig. 4.39a,b) from partial non-occlusive thrombosis (Fig. 4.39c,d). Non-occlusive thrombus may not alter the spectral Doppler flow pattern. In some instances, the head of the thrombus may float freely within the vessel lumen (Fig. 4.39e,f). This finding should be indicated in the report as it relates to an increased risk of embolism. Although many have tried to date the thrombus on the basis of its reflectivity, such attempts have been ineffective (Murphy and Cronan 1990). In chronic vein thrombosis, recanalization of the thrombus

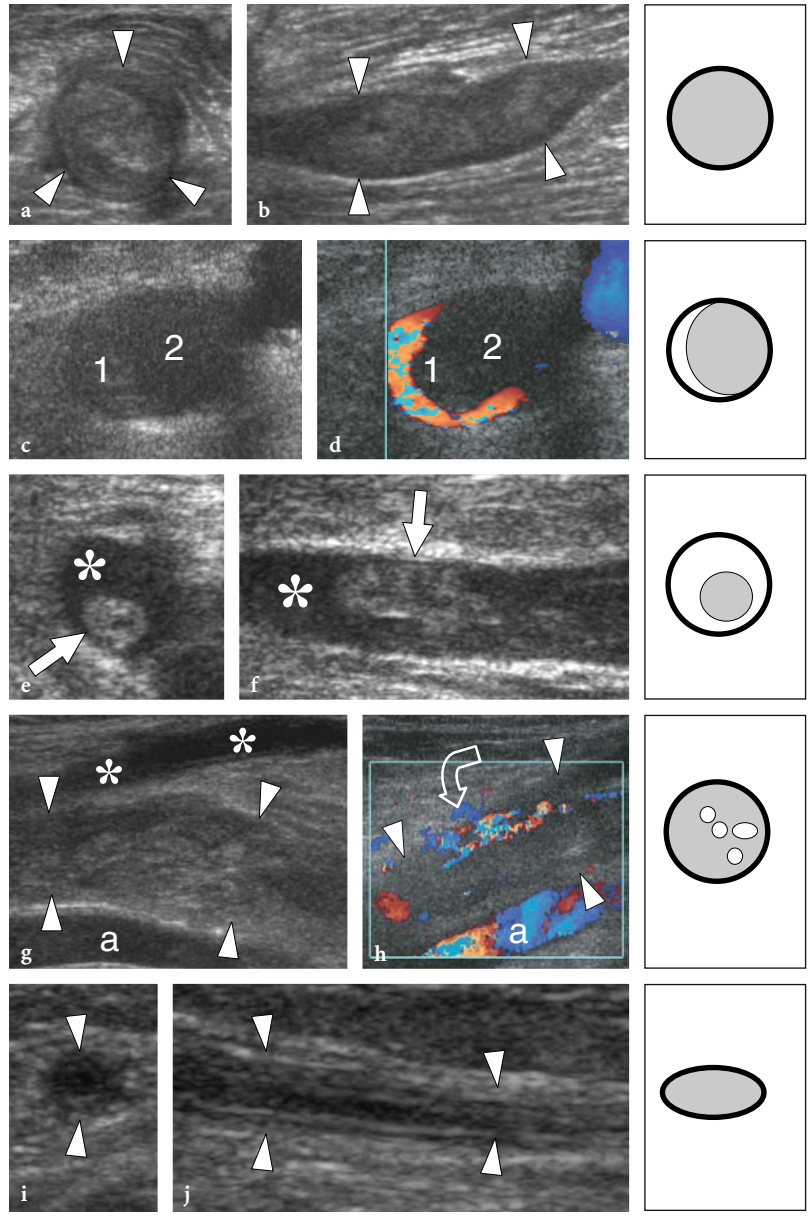

Fig. 4.39a–j. Vein thrombosis: spectrum of US appearances in different patients. **a,b** Complete vein thrombosis. **a** Short-axis and **b** long-axis 12–5 MHz US images of an intramuscular vein (*arrowheads*) of the soleus containing highly echogenic material consistent with chronic thrombus. This vein was noncompressible at US. **c,d** Partial vein thrombosis. **c** Short-axis gray-scale 12–5 MHz US image of the popliteal vein shows a distended lumen containing reflective material (*1*) suggestive of thrombosis. **d** Correlative transverse color Doppler 12–5 MHz US image confirms the presence of an area of non-occlusive thrombus with blood flow surrounding the periphery of the clot with a crescentic appearance. Note that part of the non-echogenic lumen (*2*) was also thrombosed indicating successive phases of thrombus apposition with time. **e,f** Floating thrombus. **e** Short-axis and **f** long-axis 12–5 MHz US images of the greater saphenous vein demonstrate the proximal head of the thrombus (*arrow*) floating freely in the patent vessel lumen (*asterisk*). During real-time observation, the thrombus could be seen knocking against the vessel wall. This kind of thrombus correlates with the highest risk of embolism. **g,h** Recanalized thrombus. Long-axis **g** gray-scale and **h** color Doppler 12–5 MHz US images over the posterior knee show an enlarged popliteal vein (*arrowheads*) containing heterogeneous thrombus. Tiny longitudinal hypoechoic channels with flow (*curved arrow*) are seen inside the thrombus reflecting a process of partial recanalization. Observe the popliteal artery (*a*) and superficial venous collaterals (*asterisks*). **i,j** Chronic vein occlusion. **i** Short-axis and **j** long-axis 12–5 MHz US images of the small saphenous vein demonstrate an occluded vessel (*arrowheads*) which appears markedly narrowed. The schematic drawings on the right side of the US images report the cross-sectional profile of a vein with disposition of thrombus (*gray*) and patent lumen (*white*) in relation to the different types of vein thrombosis described

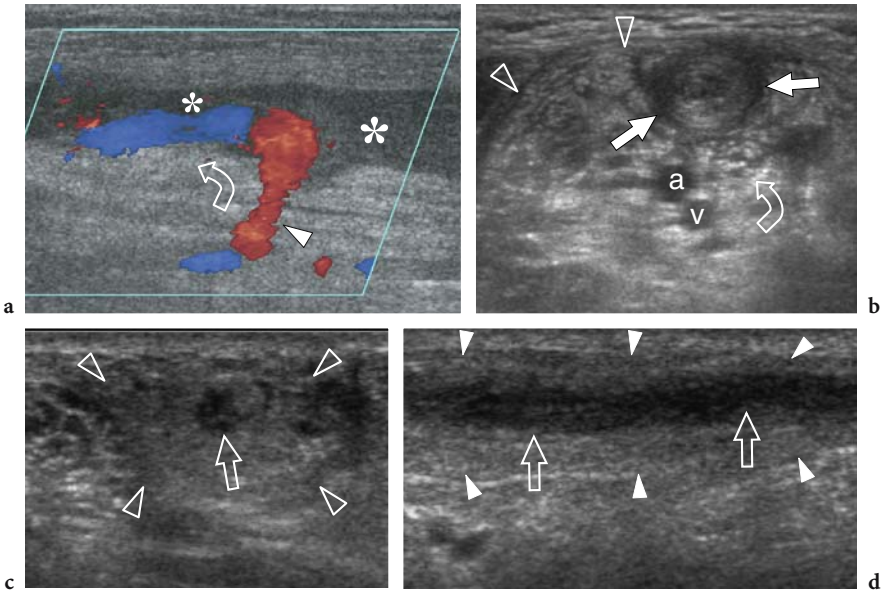

Fig. 4.40a–d. Common vascular and soft-tissue abnormalities associated with vein thrombosis. Three different cases. **a** Opening of collateral vessels. Long-axis color Doppler 12–5 MHz US image over a thrombosed greater saphenous vein (*asterisks*) demonstrates a process of partial recanalization (*curved arrow*) by a collateral vessel (*arrowhead*). **b** Muscle edema related to venous stasis. Short-axis gray-scale 12–5 MHz US image over the bicipital fossa shows a thrombosed cephalic vein (*arrows*) that lies superficial to the brachial artery (*a*), the median nerve (*curved arrow*), and a patent brachial vein (*v*). Note the subfascial edema (*arrowheads*) involving the biceps brachii muscle as a result of venous stasis. **c,d** Superficial thrombophlebitis of the lower leg. **c** Short-axis and **d** long-axis 12–5 MHz US images over a thrombosed lesser saphenous vein (*arrows*) demonstrate ill-defined vessel walls and a wide hyperechoic halo (*arrowheads*) surrounding the thrombosed vein consistent with reactive inflamed subcutaneous fat

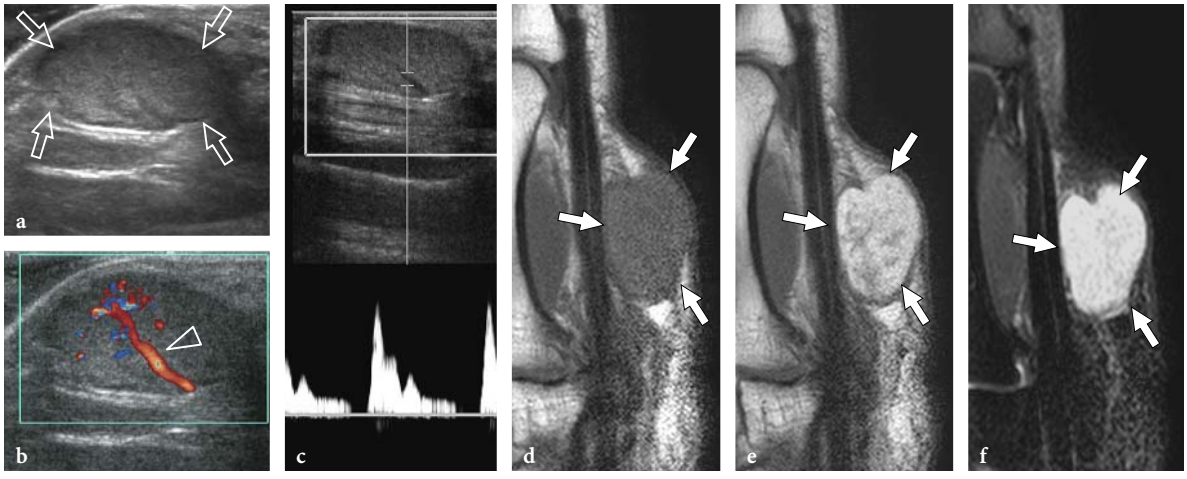

Fig. 4.41a–f. Angioleiomyoma. **a,b** Sagittal **a** gray-scale and **b** color Doppler US images of the palm demonstrates a subcutaneous sharply delineated solid hypoechoic mass (*arrows*) with a large arterial pedicle branching within (*arrowhead*). **c** Spectral Doppler analysis of intratumoral vessels shows high-resistance arterial waveforms. **d–f** Sagittal **d** T1-weighted, **e** postcontrast T1-weighted and **f** fat-suppressed T2-weighted MR imaging correlation reveal a predominantly hyperintense mass (*arrows*) in T2-signal intensity and after gadolinium administration. In the postcontrast image, small hypointense foci are visible within the tumor

may present as a network of thin hypoechoic channels of flow within the echogenic thrombus, eventually causing obvious clot resorption and reopening of the vessel (Fig. 4.39g,h). Both reduction in spontaneous flow and incomplete vein compressibility accompany these stages in the post-phlebitic limb. Collateral vessels are often seen restoring venous patency (Fig. 4.40a). If recanalization does not occur, chronically thrombosed veins are characterized by narrowed size, thickened and irregular walls and collateral vessel formation (Fig. 4.39i,j). Soft-tissue or muscle edema may be ancillary findings with vein thrombosis as a consequence of venous stasis (Fig. 4.40b). As detailed in Chapter 15, US may easily diagnose thrombophlebitis, which requires treatment with anti-inflammatory drugs and not, at least routinely, anticoagulation therapy (Fig. 4.40c,d).

4.2.4 Vascular Tumors

The most frequent vascular tumor, soft-tissue hemangioma, is not dealt with in this chapter as it has already been reported in its various forms: in Chapter 2 as part of skin and subcutaneous tissue masses, in Chapter 3 as regard its intramuscular location, and in Chapter 5 in relation to its synovial type. Similarly, the glomus tumor will be described in Chapter 11. A vascular-related tumor that has received specific attention in the US literature is angioleiomyoma (vascular leiomyoma), a rare benign histotype arising from the tunica media of the veins, composed of a conglomerate of thick-walled vessels associated with smooth muscle (Sardanelli et al. 1996; Hwang et al. 1998). It is most often found in an extremity, particularly the lower leg and the foot (50–70% of cases) (Hwang et al. 1998). Angioleiomyoma causes pain that is often related to problems with footwear and may be triggered by even light trauma. US demonstrates a sharply demarcated solid hypoechoic rounded nodule, usually less than 2 cm in diameter, with one or more arterial pedicles branching within (Fig. 4.41). Spectral Doppler analysis shows a high-resistance flow pattern (Sardanelli et al. 1996). In clinical practice, angioleiomyoma should be considered in the differential diagnosis of painful nodular lesions of the extremity. Other vascular tumors includes rare aggressive histotypes, such as hemangioendothelioma, hemangiopericytoma, and angiosarcoma, all of which are characterized by a nonspecific US appearance.

References

Altinok T, Baysal O, Karakas HM et al (2004) Ultrasonographic assessment of mild and moderate idiopathic carpal tunnel syndrome. Clin Radiol 59:916–925

Amadio PC, Reiman HM, Dobijins JH (1988) Lipofibromatous hamartoma of nerve. J Hand Surg [Am] 13:67–76

Bargfrede M, Schwennicke A, Tumani H et al (1999) Quantitative ultrasonography in focal neuropathies as compared to clinical and EMG findings. Eur J Ultrasound 10:21–29

Beekman R, Visser LH (2002) Sonographic detection of diffuse peripheral nerve enlargement in hereditary neuropathy with liability to pressure palsies. J Clin Ultrasound 30:433–436

Beekman R, Visser LH (2004) High-resolution sonography of the peripheral nervous system: a review of the literature. Eur J Neurol 11:305–314

Beekman R, Schoemaker MC, van der Plas et al (2004a) Diagnostic value of high-resolution sonography in ulnar neuropathy at the elbow. Neurology 62:767–773

Beekman R, Van del Plas JPL, Uitdehaag BMJ (2004b) Clinical, electrodiagnostic and sonographic studies in ulnar neuropathy at the elbow. Muscle Nerve 30:202–208

Beggs I (1999) Sonographic appearances of nerve tumors. J Clin Ultrasound 27:363-368

Bertolotto M, Rosenberg I, Parodi RC et al (1996) Case report: fibroma of tendon sheath in the distal forearm with associated median nerve neuropathy: US, CT and MR appearance. Clin Radiol 51:370–372

Bianchi S, Montet X, Martinoli C et al (2004) High-resolution sonography of compressive neuropathies of the wrist. J Clin Ultrasound 32:451–461

Bilge T, Kaya A, Alatli M et al (1989) Hemangioma of the peroneal nerve: case report and review of the literature. Neurosurgery 25:649–652

Bodner G, Huber B, Schwabegger A, Lutz M et al (1999) Sonographic detection of radial nerve entrapment within a humerus fracture. J Ultrasound Med 20:131–136

Bodner G, Buchberger W, Schocke M et al (2001) Radial nerve palsy associated with humeral shaft fracture: evaluation with US: initial experience. Radiology 219:811–816

Bodner G, Harpf C, Gardetto A et al (2002a) Ultrasonography of the accessory nerve: normal and pathologic findings in cadavers and patients with iatrogenic accessory nerve palsy. J Ultrasound Med 21:1159–1163

Bodner G, Harpf C, Meirer R et al (2002b) Ultrasonographic appearance of supinator syndrome. J Ultrasound Med 21:1289–1293

Buchberger W, Schon G, Strasser K et al (1991) High-resolution ultrasonography of the carpal tunnel. J Ultrasound Med 10:531–537

Buchberger W, Judmaier W, Birbamer G et al (1992) Carpal tunnel syndrome: diagnosis with high-resolution sonography. AJR Am J Roentgenol 159:793–798

Chamlou R, Stefanidis C, Lambert T et al (2002) Popliteal artery pseudoaneurysm and hereditary multiple exostoses. Acta Chir Belg 102:467–469

Chen P, Massengill A, Maklad N et al (1996) Nerve territory-oriented macrodactyly: unusual cause of carpal tunnel syndrome. J Ultrasound Med 15:661–664

Chen P, Maklad N, Redwine M et al (1997) Dynamic high-resolution sonography of the carpal tunnel. AJR Am J Roentgenol 168:533–537

Chien AJ, Jamadar DA, Jacobson JA et al (2003) Sonography and MR imaging of posterior interosseous nerve syndrome with surgical correlation. AJR Am J Roentgenol 181:219–221

Chin EE, Zimmerman PT, Grant EG (2005) Sonographic evaluation of upper extremity deep venous thrombosis. J Ultrasound Med 24:829–838

Chiou HJ, Chou YH, Cheng SP et al (1998) Cubital tunnel syndrome: diagnosis by high-resolution ultrasonography. J Ultrasound Med 17:643–648

Chong WK, Lawrence R, Gardener J (1993) The appearance of normal and abnormal arterial morphology on intravascular ultrasound. Clin Radiol 48:301–306

Chuang YM, Luo CB, Chou YH et al (2002) Sonographic diagnosis and treatment of a median nerve epineurial hematoma caused by brachial artery catheterization. J Ultrasound Med 21:705–708

Clevert DA, Rupp N, Reiser M et al (2005) Improved diagnosis of vascular dissection by ultrasound B-flow: a comparison with color-coded Doppler and power Doppler sonography. Eur Radiol 15:342–347

Cronan JJ, Dorfman GS, Scola FH et al (1987) Deep venous thrombosis: US assessment using vein compression. Radiology 162:191–194

Davison BD, Polak JF (2004) Arterial injuries: a sonographic approach. Radiol Clin North Am 42:383–396

Delfiner JS (1996) Dynamic and pathophysiology of nerve compression in the upper extremity. Orthop Clin North Am 27:219–226

Delgado GJ, Chung CB, Lektrakul N et al (2002) Tennis leg: clinical US study of 141 patients and anatomic investigation of four cadavers with MR imaging and US. Radiology 224:112–119

Duncan I, Sullivan P, Lomas F (1999) Sonography in the diagnosis of carpal tunnel syndrome. AJR Am J Roentgenol 173:681–683

Edwards JM, Zierler RE (1992) Duplex ultrasound assessment of upper extremity arteries. In: Zwiebel WJ (ed) Introduction to vascular ultrasonography, 3rd edn. WB Saunders, Philadelphia, pp 223–235

El-Karabaty H, Hetzel A, Galla TJ et al (2005) The effect of carpal tunnel release on median nerve flattening and nerve conduction. Electromyogr Clin Neurophysiol 45:223–227

El Miedany YM, Aty SA, Ashour S (2004) Ultrasonography versus nerve conduction study in patients with carpal tunnel syndrome: substantive or complementary tests? Rheumatology 43:887–895

Erickson SJ (1997) High-resolution imaging of the musculoskeletal system. Radiology 205:593–618

Eusebi V, Bondi A, Cancellieri A et al (1990) Primary malignant lymphoma of sciatic nerve: report of a case. Am J Surg Pathol 14:881–885

Foley WD, Middleton WD, Lawson TL et al (1989) Color Doppler ultrasound imaging of lower-extremity venous disease. AJR Am J Roentgenol 152:371–376

Fornage BD (1988) Peripheral nerves of the extremities: imaging with US. Radiology 167:179–182

Fornage BD, Nerot C (1987) Sonographic diagnosis of tuberculoid leprosy. J Ultrasound Med 6:105–107

Fraser JD, Anderson DR (2004) Venous protocols, techniques and interpretations of the upper and lower extremities. Radiol Clin North Am 42:279–296

Fry WR, Smith RS, Sayers DV et al (1993) The success of duplex ultrasonographic scanning in diagnosis of extremity vascular proximity trauma. Arch Surg 128:1368–1372

Gassner EM, Schocke M, Peer S et al (2002) Persistent median artery in the carpal tunnel: color Doppler ultrasonographic findings. J Ultrasound Med 21:455–461

George V, Smith AG (1996) Anatomic considerations of the peripheral nerve in compressive neuropathies of the upper extremity. Orthop Clin North Am 27:211–218

Giovagnorio F, Martinoli C (2001) Sonography of the cervical vagus nerve: normal appearance and abnormal findings. AJR Am J Roentgenol 176:745–749

Graif M, Seton A, Nerubali J et al (1991) Sciatic nerve: sonographic evaluation and anatomic-pathologic considerations. Radiology 18:405–408

Graif M, Martinoli C, Rockind S et al (2004) Sonographic evaluation of brachial plexus pathology. Eur Radiol 14:193–200

Gruber H, Peer S, Kovacs P et al (2003) The ultrasonographic appearance of the femoral nerve and cases of iatrogenic impairment. J Ultrasound Med 22:163–172

Gruber H, Peer S, Meirer R et al (2005) Peroneal nerve palsy associated with knee luxation: evaluation by sonography – initial experience. AJR Am J Roentgenol 185:1119–1125

Heinemeyer O, Reimers CD (1999) Ultrasound of radial, ulnar, median and sciatic nerves in healthy subjects and patients with hereditary motor and sensory neuropathies. Ultrasound Med Biol 25:481–485

Helvie MA, Rubin JM (1989) Evaluation of traumatic groin arteriovenous fistulas with duplex Doppler sonography. J Ultrasound Med 16:177–181

Helvie MA, Rubin JM, Silver TM et al (1988) The distinction between femoral artery pseudoaneurysms and other causes of groin masses: value of duplex Doppler sonography. AJR Am J Roentgenol 150:1177–1180

Hide IG, Grainger AJ, Naisby GP et al (1999) Sonographic findings in the anterior interosseous nerve syndrome. J Clin Ultrasound 27:459–464

Hwang JW, Ahn JM, Kang HS et al (1998) Vascular leiomyoma of an extremity: MR imaging – pathology correlation. AJR Am J Roentgenol 171:981–985

Iannicelli E, Chianta GA, Salvini V et al (2000) Evaluation of bifid median nerve with sonography and MR imaging. J Ultrasound Med 19:481–485

Ikushima K, Ueda T, Kudawara I et al (1999) Plexiform schwannoma of the foot. Eur Radiol 9:1653–1655

Isobe K, Shimizu T, Akahane T et al (2004) Imaging of ancient schwannoma. AJR Am J Roentgenol 183:331–336

Jacobs MJ, Gregoric ID, Reul GJ (1992) Profunda femoral artery pseudoaneurysm after percutaneous transluminal procedures manifested by neuropathy. J Cardiovasc Surg 33:729–731

Jacobson JA, Jebson PJL, Jeffers AW et al (2001) Ulnar nerve dislocation and snapping triceps syndrome: diagnosis with dynamic sonography – report of three cases. Radiology 220:601–605

Katsumi K, Ogose A, Hotta T et al (2003) Plexiform schwannoma of the forearm. Skeletal Radiol 32:719–723

Keberle M, Jennett M, Kenn W et al (2000) Technical advances in ultrasound and MR imaging of carpal tunnel syndrome. Eur Radiol 10:1043–1050

Kele H, Verheggen R, Bittermann HJ et al (2002) The potential value of ultrasonography in the evaluation of carpal tunnel syndrome. Neurology 61:389–391

King AD, Ahuja AT, King W et al (1997) Sonography of periph-

eral nerve tumors of the neck. AJR Am J Roentgenol 169:1695–1698
Knudson MM, Lewis FR, Atkinson K, Neuhaus A (1993) The role of duplex ultrasound arterial imaging in patients with penetrating extremity trauma. Arch Surg 128:1033–1037
Kotevoglu N, Gülbahce-Saglam S (2005) Ultrasound imaging in the diagnosis of carpal tunnel syndrome and its relevance to clinical evaluation. Joint Bone Spine 72:142–145
Koyuncuoglu HR, Kutluhan S, Yesildag A et al (2005) The value of ultrasonographic measurement in carpal tunnel syndrome in patients with negative electrodiagnostic tests. Eur J Radiology 56:365–369
Lanzillo B, Pappone N, Crisci C et al (1998) Subclinical peripheral nerve involvement in patients with rheumatoid arthritis. Arthritis Rheum 41:1196–1202
Lee D, van Holsbeeck MT, Janevski PK et al (1999) Diagnosis of carpal tunnel syndrome: ultrasound versus electromyography. Radiol Clin North Am 37:859–872
Lin J, Martel W (2001) Cross-sectional imaging of peripheral nerve sheath tumors: characteristic signs on CT, MR imaging, and sonography. AJR Am J Roentgenol 176:75–82
Lin J, Jacobson JA, Hayes CW (1999) Sonographic target sign in neurofibromas. J Ultrasound Med 18:513–517
Liskutin J, Dorffner R, Resinger M et al (2000) Hypothenar hammer syndrome. Eur Radiol 10:542
Marom EM, Helms CA (1999) Fibrolipomatous hamartoma: pathognomonic on MR imaging. Skeletal Radiol 28:260–264
Martin AJ, Ryan LK, Gotlieb AI et al (1997) Arterial imaging: comparison of high-resolution US and MR imaging with histologic correlation. RadioGraphics 17:189–202
Martinoli C, Bianchi S, Derchi LE (1999) Tendon and nerve sonography. Radiol Clin North Am 37:691–711
Martinoli C, Bianchi S, Derchi LE (2000a) Ultrasonography of peripheral nerves. Semin US CT MR 21:205–213
Martinoli C, Bianchi S, Gandolfo N et al (2000b) US of nerve entrapments in osteofibrous tunnels of the upper and lower limbs. RadioGraphics 20:199–217
Martinoli C, Derchi LE, Bertolotto M et al (2000c) US and MR imaging of peripheral nerves in leprosy. Skeletal Radiol 29:142–150
Martinoli C, Schenone A, Bianchi S et al (2002) Sonography of median nerve in Charcot-Marie-Tooth disease. AJR Am J Roentgenol 178:1553–1556
Martinoli C, Bianchi S, Prato N et al (2003) US of the shoulder: non-rotator cuff disorders. RadioGraphics 23:381–401
Martinoli C, Bianchi S, Pugliese F et al (2004) Sonography of entrapment neuropathies in the upper limb (wrist excluded). J Clin Ultrasound 32:438–450
Miller-Thomas MM, West OC, Cohen AM (2005) Diagnosing traumatic arterial injury in the extremities with CT angiography: pearls and pitfalls. RadioGraphics 25:133–142
Murphey MD, Smith WS, Smith SE et al (1999) Imaging of musculoskeletal neurogenic tumors: radiologic-pathologic correlation. RadioGraphics 19:1253–1280
Murphy TP, Cronan JJ (1990) Evolution of deep venous thrombosis: a prospective eevaluation with US. Radiology 177:543–548
Nadkar MY, Agarwal R, Samant RS et al (2001) Neuropathy in rheumatoid arthritis. J Assoc Physicians India 49:217–220
Nakamichi K, Tachibana S (1995) Restricted motion of the median nerve in carpal tunnel syndrome. J Hand Surg [Br] 20:460–464
Nakamichi K, Tachibana S, Kitajima I (2000) Ultrasonography in the diagnosis of ulnar tunnel syndrome caused by an occult ganglion. J Hand Surg [Br] 25:503–504
Okamoto M, Abe M, Shirai H et al (2000) Diagnostic ultrasonography of the ulnar nerve in cubital tunnel syndrome. J Hand Surg [Br] 5:499–502
Okereke CD, Knight S, McGowan A et al (1999) Hypothenar hammer syndrome diagnosed by ultrasound. Injury 30:448–449
Ozdemir H, Mahmutyazicioglu K, Ozkokeli M et al (2003) Pseudoaneurysm of the dorsalis pedis artery: color Doppler Sonographic and angiographic findings. J Clin Ultrasound 31:283–287
Peer S, Bodner G, Mairer R et al (2001) Examination of postoperative peripheral nerve lesions with high-resolution sonography. AJR Am J Roentgenol 177:415–419
Peer S, Harpf C, Willeit J et al (2003) Sonographic evaluation of primary peripheral nerve repair. J Ultrasound Med 22:1317–1322
Pillay PK, Hardy RW Jr, Wilbourn AJ et al (1988) Solitary primary lymphoma of the sciatic nerve: case report. Neurosurgery 23:370–371
Polak JF, Culter SS, O'Leary DH (1989) Deep veins of the calf: assessment with color Doppler flow imaging. Radiology 171:81–485
Propeck T, Quinn TJ, Jacobson JA et al (2000) Sonography and MR imaging of bifid median nerve with anatomic and histologic correlation. AJR Am J Roentgenol 175:1721–1725
Prosser AJ, Burke FD (1987) Haemangioma of the median nerve associated with Raynaud's phenomenon. J Hand Surg 12:227–228
Provost N, Bonaldi VM, Sarazin L (1997) Amputation stump neuroma: ultrasound features. J Clin Ultrasound 25:85–89
Puig S, Turkof E, Sedivy R et al (1999) Sonographic diagnosis of recurrent ulnar nerve compression by ganglion cysts. J Ultrasound Med 18:433–436
Quinn TJ, Jacobson JA, Craig JG, van Holsbeeck MT (2000) Sonography of Morton's neuromas. AJR Am J Roentgenol 174:1723–1728
Read JW, Noakes JB, Kerr D et al (1999) Morton's metatarsalgia: sonographic findings and correlated histopathology. Foot Ankle Int 20:153–161
Redd RA, Peters VJ, Emery SF et al (1989) Morton neuroma: sonographic evaluation. Radiology 171:415–417
Reynolds DL Jr, Jacobson JA, Inampudi P et al (2004) Sonographic characteristics of peripheral nerve sheath tumors. AJR Am J Roentgenol 182:741–744
Ridley DS, Jopling WH (1966) Classification of leprosy according to immunity: a five group system. Int J Leprosy 34:255–273
Rieger M, Mallouhi A, Tauscher T et al (2006) Traumatic arterial injuries of the extremities: initial evaluation with MDCT angiography. AJR Am J Roentgenol 186:656–664
Roncaroli F, Poppi M, Riccioni L et al (1997) Primary non-Hodgkin's lymphoma of the sciatic nerve followed by localization in the central nervous system: case report and review of the literature. Neurosurgery 40:618–621
Rosenbaum R (2001) Neuromuscular complications of connective tissue diseases. Muscle Nerve 24:154–169
Rossey-Marec D, Simonet J, Beccari R et al (2004) Ultrasonographic appearance of idiopathic radial nerve constriction proximal to the elbow. J Ultrasound Med 23:1003–1007
Roubidoux MA, Hertzberg BS, Carroll BA et al (1990) Color

flow and image-directed Doppler ultrasound evaluation of iatrogenic arteriovenous fistulas in the groin. J Clin Ultrasound 18:463–469
Sacks D, Robinson ML, Perlmutter GS (1989) Femoral arterial injury following catheterization: duplex evaluation. J Ultrasound Med 8:241–246
Said G, Lacroix C (2005) Primary and secondary vasculitis neuropathy. J Neurol 252:633–641
Sardanelli F, Renzetti P, Nardi F et al (1996) Imaging of angioleiomyoma. J Clin Ultrasound 24:268–271
Schenone A, Mancardi GL (1999) Molecular basis of inherited neuropathies. Curr Opin Neurol 12:603–616
Schon LC (1994) Nerve entrapment, neuropathy and nerve dysfunction in athletes. Orthop Clin North Am 25:47–59
Schwartz M, Weaver F, Yellin A et al (1993) The utility of color Doppler examination in penetrating extremity arterial trauma. Am Surg 59:375–378
Schwartz RA, Kerns DB, Mitchell DG (1991) Color Doppler ultrasound imaging in iatrogenic arterial injuries. Am J Surg 162:4–8
Shafighi M, Gurunluoglu R, Ninkovic M et al (2002) Ultrasonography for depiction of brachial plexus injury. J Ultrasound Med 22:631–634
Sheppard DG, Iyer RB, Fenstermacher MJ (1998) Brachial plexus: demonstration at US. Radiology 208:402–406
Siegel RJ, Chae JS, Maurer G et al (1993) Histopathologic correlation of the three-layered intravascular ultrasound appearance of normal adult human muscular arteries. Am Heart J 126:872–878
Silvestri E, Martinoli C, Derchi LE et al (1995) Echotexture of peripheral nerves: correlation between US and histologic findings and criteria to differentiate tendons. Radiology 197:291–296
Simonetti S, Bianchi S, Martinoli C (1999) Neurophysiological and ultrasound findings in sural nerve lesions following stripping of the small saphenous vein. Muscle Nerve 22:1724–1726
Sivri A, Guler-Uysal F (1998) The electroneurophysiological evaluation of rheumatoid arthritis patients. Clin Rheumatol 17:416–418
Sobiesk GA, Wertheimer SJ, Schulz R et al (1997) Sonographic evaluation of interdigital neuromas. J Foot Ankle Surg 36:364–366
Spinner RJ, Atkinson JL, Tiel RL (2003) Peroneal intraneural ganglia: the importance of the articular branch: a unifying theory. J Neurosurg 99:330–343
Spinner RJ, Amrami KK, Rock MG (2005) The use of MR arthrography to document an occult joint communication in a recurrent peroneal intraneural ganglion. Skeletal Radiol 35:172–179
Stewart JD (2003) Peripheral nerve fascicles: anatomy and clinical relevance. Muscle Nerve 28:525–541
Talha H, Enon B, Chevalier JM et al (1987) Brachial artery entrapment: compression by the supracondylar process. Ann Vasc Surg 1:479–482
Velling TE, Brennan FJ, Hall LD et al (2001) Sonographic diagnosis of ulnar artery aneurysm in hypothenar Hammer syndrome: report of 2 cases. J Ultrasound Med 20:921–924
Verhagen WIM, Gabreels-Festen AA, van Wensen PJ et al (1993) Hereditary neuropathy with liability to pressure palsies: a clinical, electroneurophysiological and morphological study. J Neurol Sci 116:176–184
Wilson D (2004) Ultrasound assessment of carpal tunnel syndrome. Clin Radiol 59:909
Wong BZY, Amrami KK, Wenger DE et al (2006) Lipomatosis of the sciatic nerve: typical and atypical MRI features. Skeletal Radiol 35:180–184
Wong SM, Griffith JF, Hui ACF (2004) Carpal tunnel syndrome: diagnostic usefulness of sonography. Radiology 232:93–99
Woodruff JM (1993) The pathology and treatment of peripheral nerve tumors and tumor-like conditions. Cancer J Clin 43:290–308
Wright LB, Matchett WJ, Cruz CP et al (2004) Popliteal artery disease: diagnosis and treatment. RadioGraphics 24:467–469
Yamaguchi S, Mn S, Yonemitsu Y et al (2002) A traumatic pseudoaneurysm of the dorsalis pedis artery: report of a case. Surg Today 32:756–757
Yamazaki H, Saitoh S, Seki H, et al (1999) Peroneal nerve palsy caused by intraneural ganglia. Skeletal Radiol 28:52–56
Yesildag A, Kutluhan S, Sengul N et al (2004) The role of ultrasonographic measurements of the median nerve in the diagnosis of carpal tunnel syndrome. Clin Radiol 59:910–915
Ziswiler HR, Reichenbach S, Vögelin E et al (2005) Diagnostic value of sonography in patients with suspected carpal tunnel syndrome: a prospective study. Arthritis Rheum 52:304–311